Chapter 2

THE DEFORMED STATE

2.1 INTRODUCTION

The emphasis in this and the following chapter is quite different to that of the remaining chapters of the book. The most significant of the many changes associated with recrystallization and other annealing phenomena is the decrease in the density of dislocations. In this chapter we are concerned with dislocation **accumulation** rather than dislocation **loss** and with the increases in stored energy that are a result of deformation. The dislocations provide the driving force for the annealing phenomena dealt with in the remaining chapters.

A comparison of the present chapter with those dealing with annealing will reveal discrepancies between our current knowledge of the deformed state and our requirements for the understanding of annealing. For example, we currently have an incomplete understanding of the rates of dislocation accumulation during deformation and of the large-scale deformation heterogeneities which are important in nucleating recrystallization, and this impedes the formulation of quantitative models of recrystallization. On the other hand, we now have a great deal of information about the formation of boundaries during deformation, but have not yet formulated annealing theories which adequately take these into account. Such discrepancies provide useful pointers to areas which require further research.

During deformation the microstructure of a metal changes in several ways. First, and most obvious, the grains change their shape and there is a surprisingly large increase in the total grain boundary area. The new grain boundary area has to be created during

deformation and this is done by the incorporation of some of the dislocations that are continuously created during the deformation process. A second obvious feature, particularly at the electron microscope level, is the appearance of an internal structure within the grains. This too, results from the accumulation of dislocations. Except for the small contribution of any vacancies and interstitials that may have survived, the sum of the energy of all of the dislocations and new interfaces represents the stored energy of deformation. There is one other consequence of deformation that is relevant to the study of annealing processes. During deformation the orientations of single crystals and of the individual grains of a polycrystalline metal change relative to the direction(s) of the applied stress(es). These changes are not random and involve rotations which are directly related to the crystallography of the deformation. As a consequence the grains acquire a preferred orientation, or **texture,** which becomes stronger as deformation proceeds, and this is considered in chapter 3.

Every stage of the annealing process involves loss of some of the stored energy and a corresponding change in microstructure. The release of stored energy provides the driving force for recovery and recrystallization, but it is the nature of the microstructure that controls the development and growth of the nuclei that will become recrystallized grains and also their orientation. If these changes are to be understood it is essential that we begin by examining the nature of the deformed state, the generation of microstructure and particularly the development of inhomogeneities in that microstructure. Unfortunately our knowledge of these matters is still imperfect and Cottrell's assessment of the situation some 50 years ago is still valid.

Few problems of crystal plasticity have proved more challenging than work hardening. It is a spectacular effect, for example enabling the yield strength of pure copper and aluminium crystals to be raised a hundredfold. Also, it occupies a central place in the subject, being related both to the nature of the slip process and to processes such as ***recrystallization*** *and creep. It was the first problem to be attempted by the dislocation theory of slip and may well prove the last to be solved.*

A.H. Cottrell (1953)

2.2 THE STORED ENERGY OF COLD WORK

2.2.1 Origin of the stored energy

Most of the work expended in deforming a metal is given out as heat and only a very small amount (~1%) remains as energy stored in the material. This stored energy, which provides the source for all the property changes that are typical of deformed metals, is derived from the point defects and dislocations that are generated during deformation. However, the mobility of vacancies and interstitials is so high that except in the special case of deformation at very low temperatures, point defects do not contribute significantly to the stored energy of deformation. In the common case of deformation at ambient temperatures almost all of the stored energy is derived from the accumulation of dislocations and the essential difference between the deformed and the annealed states lies in the dislocation content and arrangement. Because of this, discussion of the

significance of the deformation microstructure during recovery and recrystallization must be based on the density, distribution and arrangement of dislocations.

The increase in dislocation density is due to the continued trapping of newly created mobile dislocations by existing dislocations and their incorporation into the various microstructural features that are characteristic of the deformed state. One of the simplest of these is the grain shape. During deformation, the grains of a polycrystalline metal change their shape in a manner that corresponds to the macroscopic shape change. As a result there is an increase in grain boundary area. Consider the case of a cube-shaped grain during rolling. After 50% reduction the surface area of this grain is increased by ~16%; after 90% reduction the increase is 270% and after 99% reduction it is 3267%. The retention of contiguity requires that this new grain boundary area be continuously created during deformation and this is done by the incorporation of some of the dislocations generated during deformation.

The energy associated with this increase in area represents a significant part of the stored energy of cold working and obviously it will be greater for small grain sizes and large strains. Gil Sevillano et al. (1980) have considered the case of a severely compressed metal ($\varepsilon = 5$, i.e. reduction in thickness ~99.3%), with grain size 10 μm and cubic grains. It was assumed that the grain boundary energy remained constant at 0.7 Jm^{-2}. The energy stored in the grain boundaries under these conditions was predicted to be $\sim 10^6$ Jm^{-3}, i.e. ~71 J/mol for copper.

The rate of increase of grain boundary area per unit volume depends very much on the mode of deformation. The grains of a rolled sheet become laths, those of a drawn wire become needles and those of a compressed specimen are disc shaped. Figure 2.1 shows the calculated increase as a function of strain for several deformation modes. This increase in boundary area is an important factor in promoting continuous recrystallization after large strain deformation as discussed in chapter 14.

A second significant feature of the deformation microstructure is the appearance of an internal structure within the grains. This may take several forms but all of these involve the creation of boundaries of some sort. Many of the newly created dislocations are subsequently located in these internal boundaries. A further source of dislocations and, therefore of stored energy is associated with the presence in the metal of second-phase particles that may deform less readily or not at all. This incompatibility results in the formation of additional dislocations as discussed in §2.9.2.

In a typical lightly-deformed metal the stored energy is about 10^5 Jm^{-3}. This is a surprisingly low value. It represents only about 0.1% of the latent heat of fusion (~13 kJ/mol for the solidification of copper) and is very much smaller than the energy changes associated with phase transformations (0.92 kJ/mol for the α–γ transformation in iron). As a consequence of this, any phase transformations that may occur at the annealing temperature, e.g. precipitation of a second phase or an ordering reaction, may have a profound effect on the recrystallization behaviour. Nevertheless this small amount of stored energy is the source of all the strengthening that occurs during deformation and its loss leads to all of the property changes that occur during annealing.

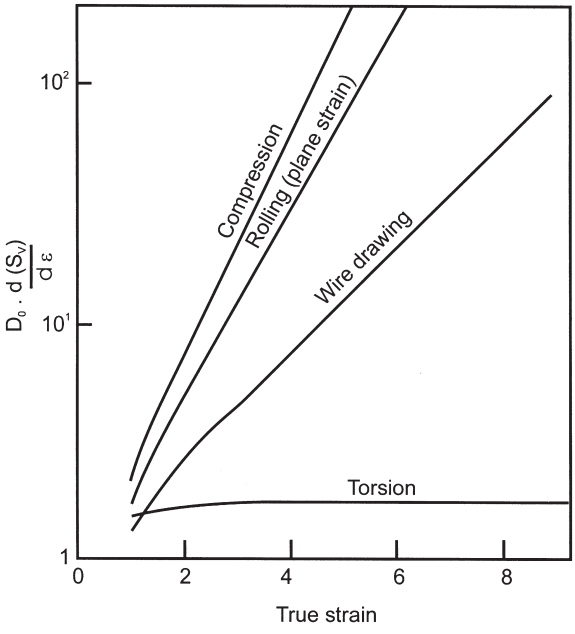

Fig. 2.1. Rate of growth of grain boundary area per unit volume (S_V) for different modes of deformation assuming an initial cubic grain of size D_0, (after Gil Sevillano et al. 1980).

The increase in dislocation density during deformation arises from both the trapping of existing dislocations and the generation of new dislocations. During deformation, the dislocations (of Burgers vector b) move an average distance L, and the **dislocation density (ρ)** is related to the true strain (ε) by

$$\varepsilon = \rho \mathrm{b} \mathrm{L} \tag{2.1}$$

The value to be attributed to L and its variation with strain are responsible for much of the uncertainty in current theories of work hardening. In some cases it is possible to define limiting values, e.g. grain size or interparticle spacing. Consideration of these has given rise to what Ashby (1970) has called **geometrically stored** and **statistically necessary** dislocations. Further consideration of the work hardening of metals is however, outside the scope of this volume.

2.2.2 Measurements of overall stored energy

The determination of stored energy is not easy. It may be measured directly by calorimetry or X-ray diffraction or determined indirectly from the change in some physical or mechanical property of the material. A summary of these techniques is given in appendix 2.

2.2.2.1 Calorimetry

A good account of the results of the extensive early calorimetric measurements can be found in Bever et al. (1973). However the magnitude of the energy change involved is so low that even the best calorimetric methods require great attention to detail. The values obtained depend on such factors as composition (particularly impurity levels), grain size, and the extent and temperature of deformation. A brief summary follows:

- Stored energy increases with strain. Typical values for copper deformed in tension at room temperature are shown in figure 9.6a.
- Variations in redundant work may produce large differences in the energy stored if the method of deformation is changed. In the case of copper, values of 3.2–5.7 J/mol for tensile deformation should be compared to 3.8–8.3 J/mol for comparable compression and ~95 J/mol for wire drawing.
- At low and medium strain levels ($\varepsilon < 0.5$) more energy is stored in fine grained material than in coarse grained. At high strain levels the energy stored is usually found to be independent of grain size, although Ryde et al. (1990) have reported a higher stored energy in copper with a coarse grain size.

The development of differential scanning calorimeters (e.g. Schmidt 1989, Haessner 1990) resulted in a renewed interest in the calorimetric measurement of stored energy, and these authors examined the energy release from several metals after deformation by torsion at −196°C. Their results are shown in figure 2.2. The low temperature peaks are associated with the loss of point defects and can be ignored for our purpose but the high temperature peaks are due to dislocation loss and recrystallization. Analysis of the

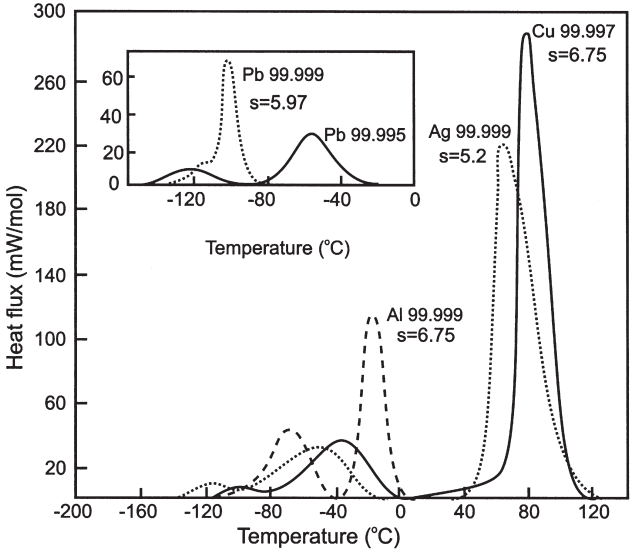

Fig. 2.2. Calorimetric readings during heating of aluminium, lead, copper and silver specimens deformed in torsion at −196°C to several different values of surface shear strain (**s**), (unpublished results of J. Schmidt, quoted by Haessner 1990).

Table 2.1
Recrystallization data for metals deformed at 77K, (Schmidt 1989).

	Al 99.999at%	Pb 99.999at%	Cu 99.997at%	Ag 99.999at%
Reduced stacking fault energy (γ_{SFE}/Gb) ($\times$1000)	26	15	4.7	2.6
Shear strain	6.75	5.97	6.75	5.2
Stored energy, J/mol	69.6	21.5	216	220
Expended energy, J/mol	3151	1400	5592	4914
E(stored)/E(expended)	0.022	0.015	0.039	0.045
Dislocation density*, m^{-2}	3.1×10^{15}	1.7×10^{15}	10×10^{15}	8.7×10^{15}

*Calculated from $[E_{stored})/Gb^2]$.

recrystallization peaks, produced the results shown in table 2.1; the magnitude of the stored energy ranges from 21.5 to 220 J/mol.

The values of stored energy for lead and aluminium are very much lower than those for copper and silver and are a direct consequence of the differences in **stacking fault energy (γ_{SFE})**. The stacking fault energy, which is related to the atomic bonding in the material, determines the extent to which unit dislocations dissociate into partial dislocations. Such dissociation, which is promoted by a low value of γ_{SFE}, hinders the climb and cross slip of dislocations, which are the basic mechanisms responsible for recovery. Dislocation theory therefore predicts that high values of γ_{SFE} should promote dynamic dislocation recovery and table 2.1 shows that γ_{SFE} for the two groups is consistent with this expectation. Attention is also drawn to the small fraction of the energy expended during deformation which is stored in the materials.

2.2.2.2 X-ray line broadening

A measure of the stored energy of a deformed metal can also be found from analysis of X-ray line broadening. This technique measures only the inhomogeneous lattice strain energy, and the difference between this and the calorimetric results provides a striking indication of the significance of the dislocation content to stored energy. The X-ray values are typically of the order of 8–80 J/mol for heavily cold worked metals in which the calorimetric value is 250–800 J/mol. The use of high intensity synchrotron X-ray sources gives more accurate results than conventional sources and more readily enables the determination of local dislocation densities as a function of grain orientation as discussed below.

2.2.3 Relationship between stored energy and microstructure

The annealing behaviour of a deformed metal is dependent not only on the overall stored energy, but more importantly on its spatial distribution. On a local scale,

inhomogeneity of stored energy will affect the nucleation of recrystallization, and larger-scale heterogeneity will influence the growth of the new grains. In order to predict the annealing behaviour, it is therefore important to determine the distribution of the defects resulting from deformation.

In this section, for the purpose of relating the microstructure and stored energy, we will assume a very simple model in which the microstructure of a polycrystal consists, in addition to the high angle grain boundaries, of only the following two components, although it will be shown in §2.4, that this is an oversimplification of the situation.

- **Cells or subgrains,** which are typically equiaxed micron-sized volumes bounded by dislocation walls. These walls are either tangled (cells) or are well-ordered low angle boundaries (subgrains). Examples of cell structures are seen in figures 2.9a and b.
- **Dislocations,** other than those which comprise the cell/subgrain boundaries.

Information about the nature and distribution of these components may be obtained experimentally using a wide variety of experimental methods, including transmission electron microscopy (TEM), X-ray diffraction, scanning electron microscopy (SEM) and electron backscatter diffraction (EBSD), as outlined in appendix 2.

2.2.3.1 Stored energy and dislocation density

In materials in which the dislocation density is low, the dislocation content may be measured directly by transmission electron microscopy. However, the density of dislocations in even moderately deformed metals is such that they cannot be counted accurately, and inhomogeneous distribution of the dislocations, for example into a cell structure, makes measurement even more difficult. An estimate of the dislocation density may also be obtained from the mechanical properties of the material. For example, a relationship between flow stress (σ) and dislocation density of the form

$$\sigma = c_1 G b \rho^{1/2} \tag{2.2}$$

where c_1 is a constant of the order of 0.5 and G is the shear modulus, has been shown to hold for a wide variety of materials (e.g. McElroy and Szkopiak 1972).

If the energy of the dislocation core is neglected and if isotropic elasticity is assumed, the energy (E_{dis}) per unit length of dislocation line is given approximately by

$$E_{dis} = \frac{G b^2 f(\nu)}{4\pi} \ln\left(\frac{R}{R_0}\right) \tag{2.3}$$

where:

R is the upper cut-off radius (usually taken to be the separation of dislocations, $\rho^{-1/2}$),
R_0 is the inner cut-off radius (usually taken as between b and 5b),
$f(\nu)$ is a function of Poisson's ratio (ν), which, for an average population of edge and screw dislocations is $\sim(1 - \nu/2)/(1 - \nu)$.

For a dislocation density ρ the stored energy is then

$$E_D = \rho E_{dis} \tag{2.4}$$

Although this relationship is appropriate if the dislocations are arranged in such a way that the stress fields of other dislocations are screened, the energies of the dislocations present in real materials are not wholly represented by such simple considerations. Dislocations in even moderately worked metals are kinked and jogged and are found in pile-ups and in intricate tangles. Dislocation theory shows that the energy of a dislocation depends on its **environment** and is for example highest in a pile-up and lowest when in a cell or subgrain wall.

In most cases where only very approximate values of dislocation energy are needed, equation 2.3 can be simplified to

$$E_{dis} = c_2 G b^2 \tag{2.5}$$

where c_2 is a constant of $\sim$0.5.

The stored energy is then given as

$$E_D = c_2 \rho G b^2 \tag{2.6}$$

The rate of storage of dislocations in the microstructure with increasing strain, is not easy to predict theoretically, and the problems in formulating models of microstructural evolution, have been reviewed by Nes (1998). If we neglect the dislocations which have created new high angle boundary (§2.2.1), the total dislocation density (ρ_{tot}) comprises those dislocations which are stored in the form of cell/subgrain boundaries (ρ_b), and those which are within the cells or subgrains (ρ_i).

Measurements of the total dislocation density in aluminium (Zehetbauer 1993), copper (Zehetbauer and Seumer 1993) and iron (Schafler et al. 1997), show that ρ_{tot} increases rapidly up to a true strain of $\sim$0.5, and thereafter increases linearly with strain, as shown in figure 2.3a. However, at larger strains, an increasing proportion of dislocations is stored in the form of cell/subgrain boundaries, and TEM measurements show that in aluminium, ρ_i increases little at strains larger than 0.3 as shown in figure 2.3b.

2.2.3.2 Stored energy and cell/subgrain structure

If the deformation microstructure consists of well-defined, equiaxed **subgrains** (§2.4.1), the stored energy may be estimated from the subgrain diameter (D) and the specific energy (γ_s) of the low angle grain boundaries which comprise the subgrain walls. The area of low angle boundary per unit volume is $\sim$3/D and hence the energy per unit volume (E_D) is given approximately by

$$E_D \approx \frac{3\gamma_s}{D} \approx \frac{\alpha \gamma_s}{R} \tag{2.7}$$

where α is a constant of $\sim$1.5.

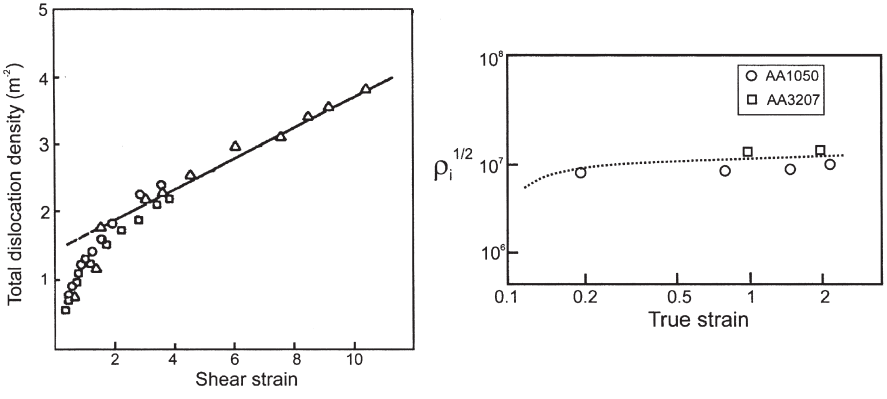

(a) (b)

Fig. 2.3 Dislocation densities in deformed metals. (a) The total dislocation density (ρ_{tot}) in deformed copper, (Zehetbauer and Seumer 1993). (b) The density of free dislocations (ρ_i) in aluminium, (Nes and Marthinsen, 2002).

As discussed in §4.3, the boundary energy (γ_s) is directly related to the misorientation (θ) across the boundary (equations 4.5 or 4.6) and therefore equation 2.7 may be expressed in terms of the parameters D and θ, both of which may be measured experimentally, as:

$$E_D = \frac{3\gamma_s\theta}{D\theta_m}\left(1 - \ln\frac{\theta}{\theta_m}\right) \approx \frac{K\theta}{D} \tag{2.8}$$

where θ_m is defined with equation 4.6 and K is a constant.

Although the use of equation 2.8 may be justified for boundaries in which the dislocation content and spacing are close to their equilibrium values, its application to less organised dislocation boundaries, such as those of cells, is unlikely to be accurate.

The cell/subgrain size – For metals deformed at room temperature, the cell/subgrain size decreases with increasing strain. Gil Sevillano et al. (1980) found that a wide range of metals exhibited a similar behaviour, which was independent of the mode of deformation, as shown in figure 2.4, and this trend has been confirmed by most later work. Nes (1998) has pointed out that above a strain of ~1, the cell sizes shown in figure 2.4 are inversely proportional to the strain.

The cell/subgrain misorientation – The variation of the orientation change across cell or subgrain boundaries with strain has not been as extensively investigated as that of the scale of the substructure. Much of the work has been carried out by diffraction in the TEM. In many cases a comparatively small number of misorientation measurements have been made, and it is unfortunate that few papers give any indication of the statistical

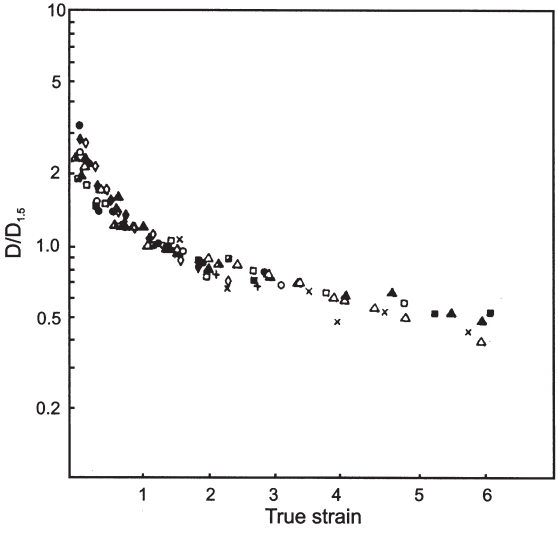

Fig. 2.4. Average cell size as a function of strain for Al, Cu, Fe, Ni, Cr, Nb, (from data assembled by Gil Sevillano et al. (1980) from different authors). The cell size is expressed as a fraction of $D_{1.5}$, the cell size at a strain of 1.5. Values of $D_{1.5}$ are Al $\sim$ 0.5 μm, Cu $\sim$ 0.3 μm, Ni $\sim$ 0.3 μm, Fe $\sim$ 0.3 μm, Cr $\sim$ 0.4 μm, Nb $\sim$ 0.2 μm.

significance of the data. EBSD measurements (appendix 2.6.1) provide data of much better statistical significance, but it is only recently that high resolution EBSD, with the capability of adequately resolving the deformed microstructures, has become available.

In their review, Gil Sevillano et al. (1980) found that the mean cell/subgrain misorientations increased with strain. However, results for aluminium alloys, summarised by Nes (1998) indicated that the misorientation saturated at $\sim$2–3° at strains of $\sim$1. This is contradicted by the TEM results on aluminium (Liu and Hansen 1995) and nickel (Hughes and Hansen 2000) shown in figure 2.5a and by the EBSD measurements of Hurley and Humphreys (2003) (fig. 2.5b), all of which show misorientations increasing with strain, and do not include misorientations associated with large scale deformation bands. The misorientations associated with more specific types of cell/subgrain boundary will be discussed in §2.4.2.

Orientation gradients – The mean subgrain misorientation is only one of the parameters describing the variation of orientation within a grain. Of particular importance for the **nucleation** of recrystallization (§7.6) are the **long range orientation gradients** in the material. In many cases it is found that although the nearest-neighbour misorientations are low, there may be significant orientation gradients within a grain, and the orientation gradient, $\Omega = d\theta/dx$, can be defined as the rate of accumulation of misorientation across some region of the microstructure (Ørsund et al. 1989). However, because of the complexity of deformed microstructures, such a concept is generally only

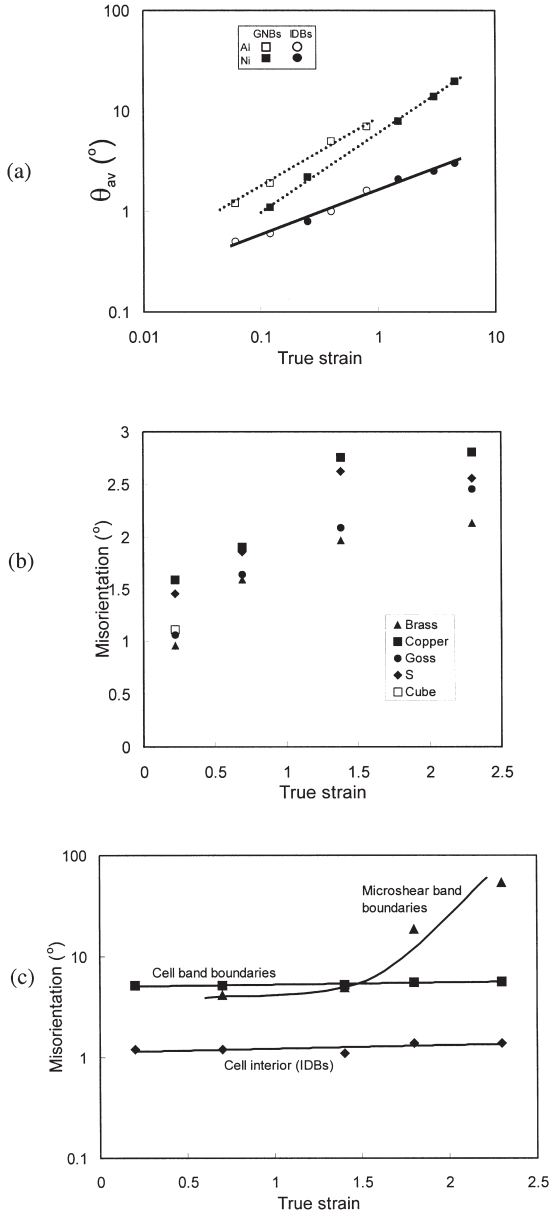

Fig. 2.5. The effect of strain on boundary misorientations in aluminium. (a) The misorientation of incidental dislocation boundaries (IDBs) and geometrically necessary boundaries (GNBs) in aluminium and nickel, (Hughes 2001). (b) The effect of grain orientation on cell misorientations in Al–0.1%Mg, (Hurley and Humphreys 2003). (c) The effect of strain on the mean misorientations of cell, cell-band and microshear-band boundaries in Al–0.1%Mg, (data from Hurley and Humphreys (2003).

useful when applied to specific microstructural features such as the regions adjacent to second-phase particles (§2.9.3) or transition bands (§2.7.3).

2.2.3.3 Orientation dependence of stored energy

It has been found experimentally that both the cell/subgrain size and the misorientation may be dependent on the grain orientation, and therefore, from equation 2.7, we expect the stored energy to vary in the different **texture components** of the material. As will be discussed later, this may have important implications for the recrystallization behaviour. The pioneering work in this area was a study of 70% cold rolled iron by Dillamore et al. (1972). At this level of rolling the microstructure consists mainly of a cell-type structure and it was found that the cell size and the misorientation between neighbouring cells were orientation dependent (fig. 2.6). For the $\{hkl\}<110>$ components of the rolling texture, small cells and large misorientations were associated with rolling plane orientations near {110}, while larger cells and small misorientations occurred for {001} orientations. From equation 2.8 it is seen that if the dislocations are concentrated mainly in cell or subgrain walls then the stored energy should be greatest for small cells and large misorientations, and Dillamore et al. concluded that

$$E_{110} > E_{111} > E_{112} > E_{100}$$

This result has proved to be very useful in providing understanding of the recrystallization textures found in low carbon steels. Every and Hatherly (1974), using the X-ray line broadening method found, in a 70% rolled, killed steel, a similar orientation dependence of the stored energy to that calculated by Dillamore et al. (1972), and their data are included in figure 2.7 which shows results from several

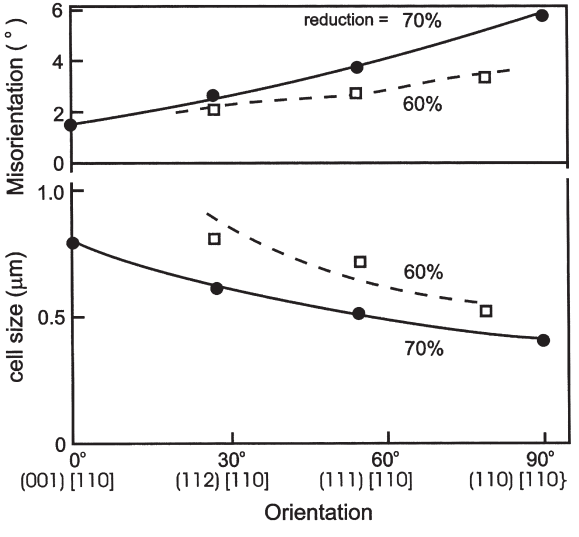

Fig. 2.6. Variation of cell size and cell boundary misorientation in rolled iron as a function of local orientation, (after Dillamore et al. 1972).

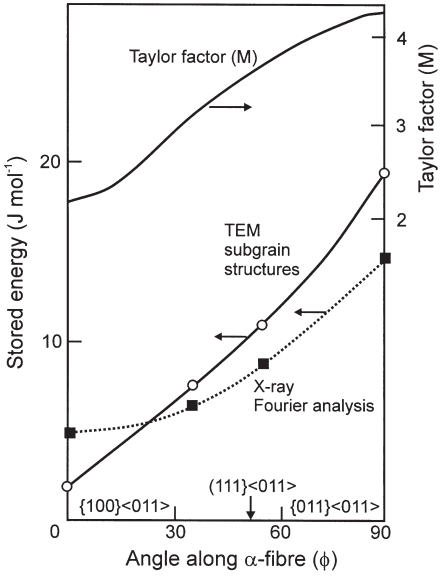

Fig. 2.7. Stored energies of deformation for different orientations in the α-fibre of cold-rolled iron and steel. TEM results from Dillamore et al. (1967) and X-ray Fourier analysis from Every and Hatherly (1974). Also shown is the variation of the Taylor factor (M), (Hutchinson 1999).

investigations of the effects of local orientation on stored energy in rolled iron and low carbon steel. These workers also examined the microstructures of their specimens and found that the predominant, high energy components ($\{110\}<uvw>$ and $\{111\}<uvw>$) consisted of cells elongated in both the transverse and rolling directions. These cells were 0.15–0.20 μm thick, 2–3 times longer, and had orientations within 10° of a $<110>$ zone between $\{110\}$ and $\{111\}$. The other, low energy components ($\{211\}<uvw>$ and $\{100\}<uvw>$) were associated with larger equiaxed cell structures of diameter 0.30–0.45 μm, and orientations lying in zones within 30° of $\{100\}$. Similar results were obtained by Willis and Hatherly (1978) from an interstitial-free (IF) steel, and recent neutron diffraction (Rajmohan et al. 1997) and synchrotron diffraction measurements (Borbely and Driver 2001) of stored energy are also in agreement with the earlier results. The effect of grain orientation on stored energy in iron and steel is well summarised in figure 2.7 (Hutchinson 1999), where it is seen to correlate with the Taylor factor (§3.7.1.2). If it is assumed that the total amount of slip activity in a grain is dependent on the Taylor factor, then such a correlation is to be expected.

There is less information on the effect of grain orientation on cells or subgrains in aluminium deformed at ambient temperatures. However, Hurley and Humphreys (2003) have recently found that although the subgrain size shows little orientation dependence, the mean subgrain misorientations show an orientation dependence as seen in figure 2.5b. Such a dependence is consistent with the trends found during high temperature deformation and shown in table 13.1.

2.2.3.4 Modelling the stored energy

Models for the increase in stored energy with strain have been reviewed by Nes (1998). The model of Nes and colleagues (Nes 1998, Nes and Marthinsen 2002) simplifies microstructure to three parameters, the cell size, the dislocation density within the cells, and the thickness of the cell walls, a parameter which decreases with increasing strain, as cells tend to become subgrains. Although such models have been developed primarily to account for the work hardening of metals, they are potentially useful for modelling the driving pressure for recrystallization.

2.3 CRYSTAL PLASTICITY

2.3.1 Slip and twinning

In cubic metals the two basic methods of deformation are **slip** and **twinning** and the most significant material parameter with respect to the choice of method is the value of the **stacking fault energy** (γ_{SFE}). In metals with a low value of γ_{SFE}, the difficulty of cross-slip reduces the ability of the material to change its shape during plastic deformation by slip alone, and therefore deformation twinning may occur.

The planes and directions of both processes are a function of the crystal structure and tables 2.2 and 2.3 show these data for cubic metals. As shown by table 2.2 the crystallography of slip in fcc metals is simple. In most cases slip takes place on the most densely packed planes and in the most densely packed directions. Together these factors define the slip system, $\{111\}<110>$. It has been known for many years however, that

Table 2.2
Crystallography of slip in cubic metals.

Structure	Slip system	
	Plane	Direction
fcc	{111}	<110>
bcc	{110}	<111>
	{112}	<111>
	{123}	<111>

Table 2.3
Crystallography of twinning in cubic metals.

Structure	Twinning shear	Twinning plane	Twinning direction
fcc	0.707	{111}	<112>
bcc	0.707	{112}	<111>

other systems sometimes operate at high temperatures and particularly in metals with high values of $\gamma_{SFE,}$ the systems observed involving slip on {100}, {110}, {112} and {122} planes (Hazif et al. 1973). More recently, the operation of such **non-octahedral slip** in aluminium at high deformation temperatures, which is inferred from surface slip markings (Maurice and Driver 1993), has been shown to influence the development of microstructures and textures (§13.2.4). Unusual, low-temperature slip has also been reported on {111}, {110} and {122} planes and Yeung (1990) has observed slip on a number of non-octahedral planes in the low stacking fault energy alloy 70:30 brass at high values of strain. For summaries of recent work in this area the reader is referred to the papers of Bacroix and Jonas (1988), Yeung (1990) and Maurice and Driver (1993).

In bcc metals slip occurs in the close packed $<111>$ directions but the slip plane may be any of the planes {110}, {112} or {123}; each of these planes contains the close packed slip direction, $<111>$. The choice of slip plane is influenced by the temperature of deformation. At temperatures below $T_m/4$ {112} slip occurs; between $T_m/4$ and $T_m/2$ {110} slip is favoured and at temperatures above $T_m/2$ {123} is preferred. At room temperature iron slips on all three planes in a common $<111>$ direction and the term pencil glide is used to describe the nature of the slip process in this case. One consequence of such slip is the wavy nature of the slip lines seen on pre-polished surfaces of deformed specimens.

In general, bcc metals deform by slip, as do fcc metals with medium to high values of γ_{SFE} such as copper ($\sim$80 mJm^{-2}) and aluminium ($\sim$170 mJm^{-2}). In metals with low values of γ_{SFE} such as silver or in alloys like 70:30 brass and austenitic stainless steels with γ_{SFE} $\sim$20 mJm^{-2}, the dislocations dissociate to form stacking faults, and twinning is the preferred mode of deformation. The tendency to deform by twinning is increased if the deformation temperature is lowered or the strain rate increased.

In polycrystalline hexagonal metals deformation begins by slip but, because of the lack of sufficient slip systems to accommodate the imposed strain, slip is soon accompanied by twinning as an important deformation mode.

2.3.2 Deformation of polycrystals

The actual planes and directions associated with slip and twinning correspond to the system with the greatest resolved shear stress and are differently oriented from grain to grain in polycrystalline metals. In general, slip or twinning processes initiated in one grain are confined to that grain and can readily be distinguished from those occurring in neighbouring grains. It should not be thought however, that deformation is homogeneous in any grain of the aggregate. When a single crystal specimen is deformed it is usually free to change its shape subject only to the need to comply with any external constraints (e.g. grip alignment in a simple tension test). This freedom does not exist for the individual grains of an aggregate which are subjected to the constraints exercised by every one of several neighbours each of which is deforming in a unique manner. It will be obvious that contiguity must be maintained if deformation is to continue and it is a direct consequence of this need that the deformation processes will

Table 2.4
Stacking fault energy of metals, (Murr 1975).

Metal	γ_{SFE} (mJm^{-2})	Metal	γ_{SFE} (mJm^{-2})
Aluminium	166	Zinc	140
Copper	78	Magnesium	125
Silver	22	91Cu:9Si	5
Gold	45	Zirconium	240
Nickel	128	304 Stainless steel	21
Cobalt (fcc)	15	70Cu:30Zn	20

be different in various parts of any particular grain, leading to the development of **microstructural inhomogeneity.**

The imposed deformation strain and the constraints between neighbouring grains affect the choice and number of the operating slip systems, and with respect to the subject of this book, there are two important consequences of this slip activity:

- The slip processes and their variation both within and between grains, largely determine the **deformation microstructures,** discussed in this chapter.
- The changes in orientation which are a consequence of the crystal plasticity, determine the **deformation textures,** discussed in chapter 3.

Theories and models of crystal plasticity – have been developed for many years. Although these can now provide good predictions of the development of deformation textures (§3.7), they have not been very successful in modelling the development of the complex microstructures discussed later in this chapter. This is largely due to the scale of the problem. The microstructures are generally too large and complex to be accounted for by dislocation theory, but are on too small a scale to be successfully modelled by finite element (FE) methods. Although crystal plasticity has been successfully incorporated into FE models (Sarma and Dawson 1996, Bate 1999, Dawson et al. 2002), and can predict some aspects of large-scale deformation heterogeneity, significant improvements need to be made before these models can account for the formation of deformation heterogeneities in sufficient detail to assist in the understanding of the nucleation of recrystallization.

It is because of their primary relevance to the formation of deformation textures that we have opted to discuss the various **theories of crystal plasticity** in chapter 3.

2.4 CUBIC METALS WHICH DEFORM BY SLIP

Metals of high or moderate stacking fault energy such as aluminium alloys, α-iron, nickel and copper deform by slip. In most cases the deformation is heterogeneous, and because crystals generally change orientation during deformation, as discussed

in chapter 3, regions of different orientation develop within the original grains. This **grain subdivision** or **fragmentation,** has been recognised for many years, but it is only recently that many aspects of the resulting microstructures have become reasonably clear. It is now known that there is a wide range of length scales, from nanometres to millimetres, at which the microstructure is subdivided during deformation, and we will first consider the various microstructural features which constitute this scale-based hierarchy, before discussing the ways in which the microstructures evolve with strain. It should be recognised that despite a very large body of literature on this subject in the past 20 years, many aspects remain unclear.

Much recent work has shown that many deformed metals develop rather similar types of microstructures, and that these change in a similar way with increasing strain. If the relationships between some of these microstructural features were to obey simple laws, it would be easier to model microstructural development, and because of this, there has been significant interest in examining **similitude** and **scaling** of deformation microstructure.

An inverse relationship between cell size (D) and strain (ε), which can be scaled to fit most metals has already been noted in §2.2.3.2. An inverse relationship between the cell size (D) and the square root of dislocation density inside the cells (ρ_i) is often found during high temperature deformation (equation 13.9), and a similar relationship has also been found after low temperature deformation of copper and iron (Staker and Holt 1972). However, it has been shown that in aluminium, this relationship breaks down for $\varepsilon > 0.3$, when ρ_i tends to saturate (Nes and Saeter 1995, Nes 1998).

Similitude in the development of boundary separations, misorientations and misorientation distributions with strain has also been reported for deformation-induced boundaries (see §2.4.1), and is reviewed by Hughes (2002).

2.4.1 The microstructural hierarchy

In this section we summarise the main features of the microstructures in deformed metals of medium and high stacking fault energy, and it is convenient to classify the microstructures according to the scale of the heterogeneity as shown schematically in figure 2.8, for a sample deformed in plane strain compression. Further details of these features and their formation during deformation are discussed in subsequent sections.

Dislocations – Dislocations may exist as tangles or other rather random structures (fig. 2.8a), particularly after low strains, as discussed in §2.2.3. In metals which do not form cells, such diffuse arrangements of dislocations are found even after large strains as discussed in §2.4.3.

Cells and subgrains – In many metals, the majority of the dislocations produced on deformation form the boundaries of cells or subgrains (fig. 2.8b), which are the smallest volume elements in the deformed microstructure. Their character and dimensions were discussed in §2.2.3, and TEM micrographs of cells in deformed copper are shown in figures 2.9a and b. Some cell walls may be aligned or have different misorientations, and this enables further sub-classification of these features as discussed in §2.4.2.

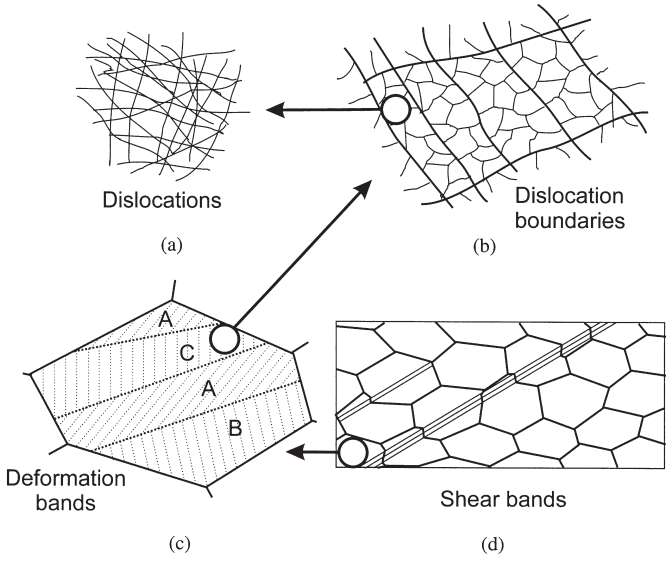

Fig. 2.8. The hierarchy of microstructure in a polycrystalline metal deforming by slip. The various features are shown at increasing scale: (a) Dislocations, (b) Dislocation boundaries, (c) Deformation and transition bands within a grain, (d) Specimen and grain-scale shear bands.

Deformation and transition bands – It is often found that individual grains within the sample, particularly in coarse-grained materials, subdivide on a large scale during deformation (fig 2.8c) into regions of different orientation, as a consequence of either inhomogeneous stresses transmitted by neighbouring grains or the intrinsic instability of the grain during plastic deformation. The resulting **deformation bands** deform on different slip systems and may develop widely divergent orientations. The narrow regions between the deformation bands, which may be either diffuse or sharp, are termed **transition bands.** Examples of deformation bands in α-brass and aluminium are shown in figures 2.9c and d.

Shear bands – Figure 2.8d shows a polycrystalline sample in which intense shear has occurred on planes inclined to the rolling plane. These shear bands, which are non-crystallographic in nature, may pass through several grains, and even extend through the specimen. They are a result of plastic instability, and can be thought of as the rolling equivalent of the 'necking' which occurs in a tensile test. Examples are seen in figures 2.9e and f.

2.4.2 The evolution of deformation microstructure in cell-forming metals

Many aspects of the formation of the larger-scale features of the microstructure, such as deformation bands and shear bands are common to most metals, and will be discussed

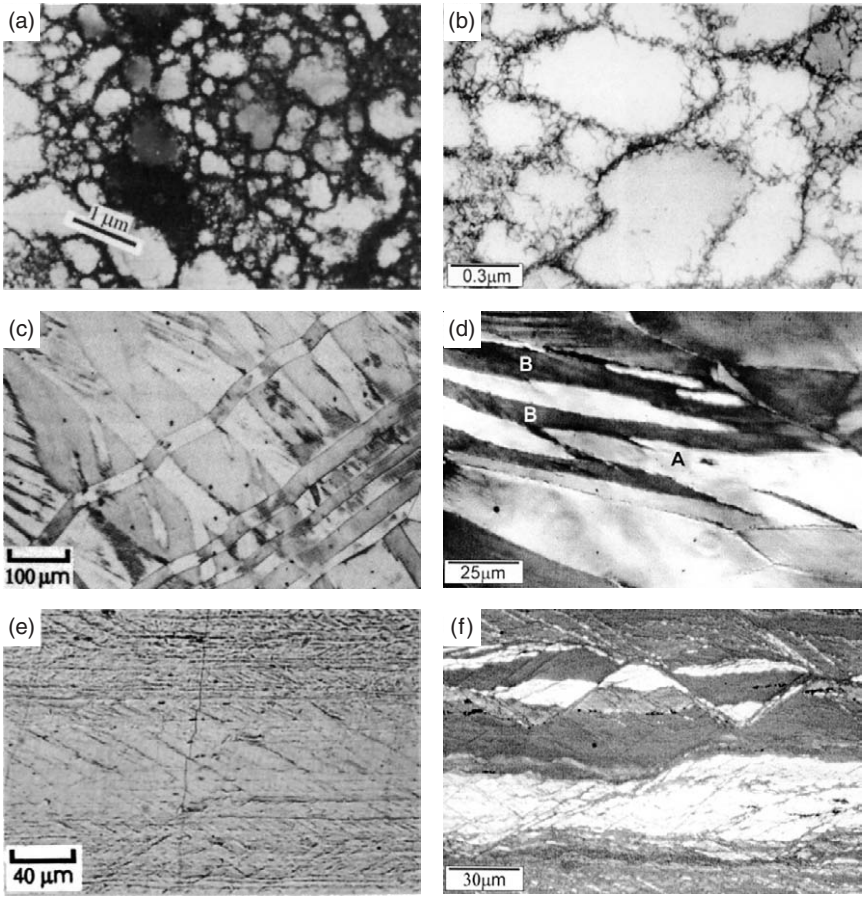

Fig. 2.9. Various features of deformed microstructures; (a) Cell structure in 25% cold rolled copper (micron bar shown), (b) Details of cell structure, (c) 70:30 brass compressed 12%, showing deformation bands, (d) Deformation bands (B) in a grain (A) in Al–1%Mg, (e) Shear bands developed by light rolling on pre-polished, and lightly scratched, surface of 83% cold rolled copper, (Malin and Hatherly 1979), (f) Shear bands in Al–Zn–Mg alloy cold rolled 90%, (courtesy of W.B. Hutchinson).

in §2.7 and §2.8 respectively. In this section we consider only the evolution of the microstructure at the cell/subgrain level shown in figure 2.8b.

During the past 20 years, there has been a surprising amount of interest in the detailed characterisation of the cell and subgrain structures formed during the deformation of fcc metals, particularly aluminium and nickel, at ambient temperatures. Much of this research stems from the group at Risø, led by Hansen. Recent discussions of this research include Hughes and Hansen (1997), Hansen and Juul Jensen (1999) and Hughes (2001).

2.4.2.1 Small strainzs ($\varepsilon < 0.3$)

Random distributions of dislocations are rarely observed in cell-forming metals. Although the slip process tends to produce high densities of dislocations on the active slip planes, energy considerations (e.g. Kuhlmann-Wilsdorf 1989) promote relaxation into boundaries by dynamic and/or static recovery. The balance between these two processes, which is affected by the nature of the material and the deformation temperature, determines the degree to which the deformed microstructure exhibits crystallographic alignment and whether the boundaries are diffuse (cells) or sharp (subgrains).

Cell formation – As shown schematically in figure 2.8b and in the TEM micrograph of figure 2.10, we can distinguish between at least two types of cell or subgrain boundary. There are **small (0.5–1 μm), approximately equiaxed cells separated by small ($\sim$1°) misorientations.** The size, shape and misorientation of these cells does not change very much during deformation (figs 2.4 and 2.5) and it is therefore thought that these cell boundaries are **transient** features of the microstructure, being the result of a dynamic balance between dislocation annihilation and trapping. The overall cell sizes shown in figure 2.4 include all low angle boundaries. However, if the various types of boundary are measured separately, the cell size in aluminium is found to initially decrease with increasing strain (ε) to $\sim$0.5 μm, but to remain almost constant at $\varepsilon > 0.5$ (Hughes 2001, Hurley and Humphreys 2003). The term **incidental dislocation boundaries (IDBs)** has been used to describe such boundaries (Kuhlmann-Wilsdorf and Hansen 1991), which are then distinguished from the higher angle, and often aligned, **geometrically necessary boundaries (GNBs)** which are discussed below. However, although we will make some use of this terminology in referring to the published literature, we do not find this a helpful classification.

We consider that it is the **transient** or **persistent** nature of boundaries which is most important in microstructural evolution, and that this characteristic differentiates these *transient* cell boundaries from other *persistent* deformation-induced boundaries, and from *persistent* features such as microshear or transition bands.

Cell blocks and cell bands – In both aluminium and nickel, the cells may occur in blocks as shown schematically in figure 2.8b (Bay et al. 1992). It is thought that the slip activity is similar within individual blocks, but differs between the blocks. In this way, each cell block can deform relatively homogeneously on less than the five slip systems required by plasticity theory (Taylor 1938) (§3.7.1.2), and the overall strain is then accomplished by the variation of slip activity between the blocks. A TEM micrograph and accompanying sketch, showing a typical arrangement of cell blocks is shown in figure 2.10. As seen in figure 2.10, the cell blocks are elongated, and a little more than one cell in width. This is typical of most deformed microstructures in aluminium, and these features are often better described as **cell bands.**

The cell blocks or bands are bounded by longer, aligned boundaries, which have been termed **dense dislocation walls** (DDWs), **microbands,** or **cell-band walls.** These are of higher misorientation angle than the boundaries within the cell blocks (Liu and Hansen 1995, Hughes and Hansen 2000, Hughes 2001, Hurley and Humphreys 2003), as shown in figures 2.5a and c. The misorientations across alternate cell-band walls tend to oscillate about a mean, with no substantial long range orientation gradient.

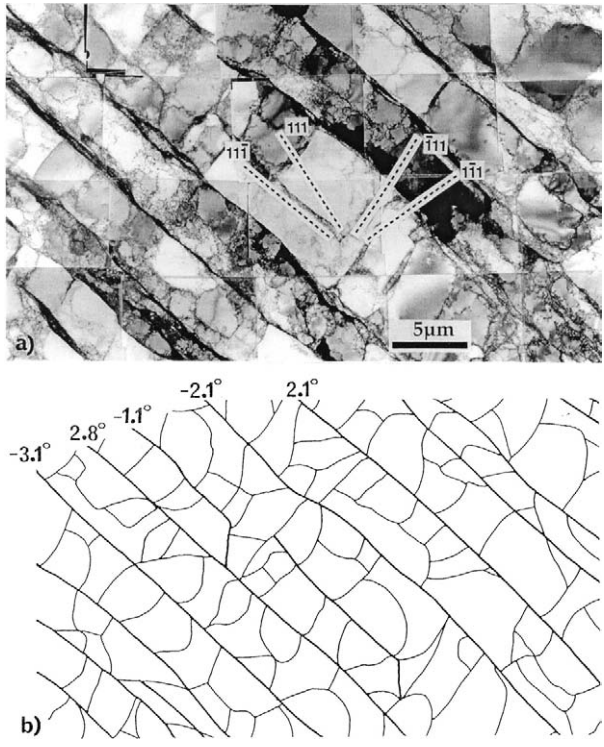

Fig. 2.10. TEM micrograph (a) of cell block structure in 10% cold rolled aluminium (ND-RD plane) and sketch (b) of the area showing the misorientations across the cell block boundaries (heavy lines), (Liu et al. 1998).

These boundaries have been termed **geometrically necessary boundaries (GNBs)** (Kuhlmann-Wilsdorf and Hansen 1991), because they accommodate the misorientations between blocks of material of different orientation. However, this term is misleading because even the small cells of low misorientation discussed above are also *geometrically necessary* at a smaller scale. If this were not so, these cell boundaries would disappear on annealing, whereas they recover to form well-organised low angle subgrain boundaries as seen in figure 6.13.

If the cell-band boundaries (GNBs) are distinguished from the cell boundaries (IDBs), as shown in figure 2.5a, it is seen that the cell-band boundary misorientations increase substantially with increasing strain. However, if the cell-band boundaries are further distinguished from **microshear-band** boundaries (another class of aligned boundary which appear at larger strains and are discussed in §2.4.2.2), their misorientations appear to remain relatively constant in aluminium, as seen in figure 2.5c.

The alignment of the boundaries – In a sample deformed in plane strain compression, the long microband or cell-band boundaries are aligned approximately parallel to the transverse direction and at an angle of 25–40° to the rolling plane. In most grains only

one strong set of microbands is seen, but in some cases two are formed. These are the planes of high shear stress, and are similar to those on which shear bands form (§2.8). In some cases the alignment in fcc metals deformed by rolling is close to {111} slip planes and in other cases it is not (e.g. Liu et al. 1998, Hansen and Juul Jensen 1999, Hurley and Humphreys 2003). However, the detailed analysis of Hurley et al. (2003) has established that the alignment in cold rolled polycrystalline aluminium is related to the deformation geometry and that any crystallographic alignment is coincidental. However, some evidence of crystallographic alignment of the boundaries has been found for samples deformed in tension (Winther et al. 2000), and these authors have shown that the nature of the alignment is influenced by the grain orientation. The alignment is clearly linked to strong slip activity, and is presumably also influenced by dynamic recovery. In polycrystals deformed at elevated temperatures where similar aligned bands form, there is no indication that the alignment is crystallographic (§13.2.3).

The microstructures discussed above have been investigated most extensively in aluminium and nickel, but rather similar structures have been reported in copper and iron. In copper rolled to low strains, the microstructure consists mainly of cells, but long, thin plate-like microbands 0.1 to 0.3 μm thick, initially aligned on {111} planes are seen (Bourelier and Le Héricy 1963, Malin and Hatherly 1979, Hatherly 1980) as shown in figure 2.11a. These appear to be similar to the crystallographically aligned microbands discussed above. Because there is much less dynamic recovery in copper than in aluminium, it is to be expected that more alignment of dislocations on active {111} slip planes will be retained in copper.

2.4.2.2 Moderate strains ($0.3 < \varepsilon < 1$)

At larger strains, the aligned cell-band structures of figure 2.10 are often intersected by thin shear bands within the grains (Hughes and Hansen 1993, Rosen et al. 1995), examples of which are shown in figure 2.12. Because these shear the elongated cell-bands into an '**S**' shape, they have been termed 'S-bands'. However, as this may cause some confusion with bands of material of the 'S-orientation', we prefer to use the term **microshear** bands. If the boundaries and not the dislocations are of primary interest, there are many benefits of using high resolution EBSD rather than TEM to investigate the deformed microstructures in aluminium (Hurley and Humphreys

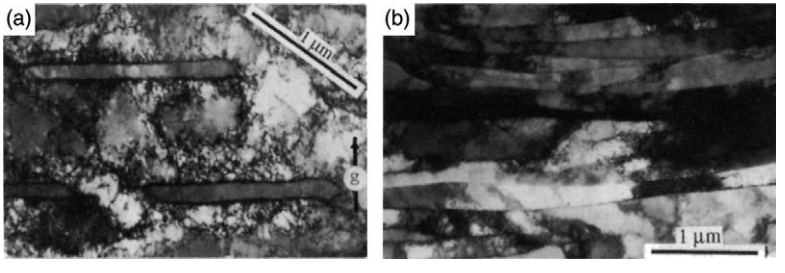

Fig. 2.11. TEM micrographs cold rolled copper. (a) Microbands in 18% rolled material, (b) Microbands in 98% rolled material. The specimen plane is ND-RD, and a 1 μm bar parallel to RD is shown, (Malin and Hatherly 1979).

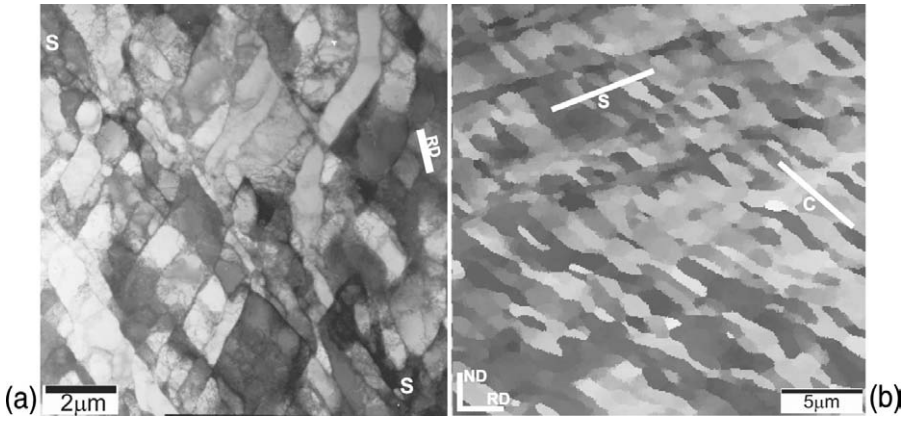

Fig. 2.12. Microstructure in ND-RD plane of Al-0.1%Mg, cold-rolled 50%, showing the interaction of the microshear bands and aligned cell bands. (a) TEM micrograph, showing microshear band **S-S** shearing the cell bands. (b) EBSD map in which the colours represent orientations, showing the cell bands (C) and microshear bands (S). The regions within the microshear bands are seen to have similar orientations, (Hurley and Humphreys 2003). (See colour plate section for fig. 2.12b).

2002, 2003), because much larger areas can be examined and quantitatively analysed. Figure 2.12b shows microshear boundaries intersecting the cell-bands in aluminium. The microshear bands are typically 1–2 μm thick and contain cells of a similar size and misorientation to the cell-bands. With increasing strain, the regions within these microshear bands become progressively misoriented from the cell-bands as shown in figure 2.5c, indicating that the shearing remains operative. The microshear bands seen in aluminium appear to be very similar to those reported for copper (Malin and Hatherly 1979).

2.4.2.3 Large strains ($\varepsilon > 1$)

With increasing strain, the microshear bands and the cell-bands become more closely aligned with the rolling plane, and at $\varepsilon > 2$ the various bands cannot be clearly identified, and at this stage, the microshear band walls have become high angle boundaries as seen in figure 2.5c. The rolled microstructures then consist almost entirely of long lamellar boundaries, many of them high angle, aligned parallel to the rolling plane, as shown in figure 2.11b. Rather similar structures of this type are found in aluminium, nickel, copper and iron, and in the latter, there is evidence (Every and Hatherly 1974) that the extent of formation of the lamellar boundary structures is dependent on orientation.

Because the annealing behaviour of alloys deformed to very large strains (>3) may be significantly different from that of materials deformed to lower strains, we give some further consideration to large strain deformation in §14.3.

2.4.2.4 Summary

We have highlighted three microstructural features – cells, cell-bands (microbands), and microshear (S) bands, and the effect of strain on the misorientations across these boundaries in aluminium is shown in figure 2.5c. Additional information about the way in which the microstructure evolves may be obtained by examining the effect of strain on the alignment of these boundaries with the rolling plane as shown for aluminium in figure 2.13.

Cells – The cell size, shape and boundary misorientation changes little with strain, which is consistent with these boundaries being **transient** features of the microstructure.

Cell-band walls – The misorientations of the cell-band (microband) walls changes very little with strain, and for $\varepsilon < 1.5$, figure 2.13 shows that there is little change in their alignment with the rolling plane. The significance of this may be seen by comparison with the change of alignment which would be found for rigid body rotation of passive features in the microstructure. These two factors suggest that at moderate strains the cell-bands or microbands are also **transient** microstructural features which may migrate or re-form during the deformation, up to $\varepsilon \sim 1.5$. Above this strain, the bands undergo rigid body rotation, suggesting that they are no longer active, and have become **persistent** microstructural features.

Microshear bands – In microshear (S) bands the misorientations across the walls increase with increasing strain (fig. 2.5c), and the walls are seen from figure 2.13 to rotate at a rate consistent with a rigid body. This suggests that once formed, these features are permanent features of the microstructure, although the shear within them, and the misorientations across them, increase with strain. This observation is consistent with the earlier observations of Malin and Hatherly (1979) on similar bands in copper.

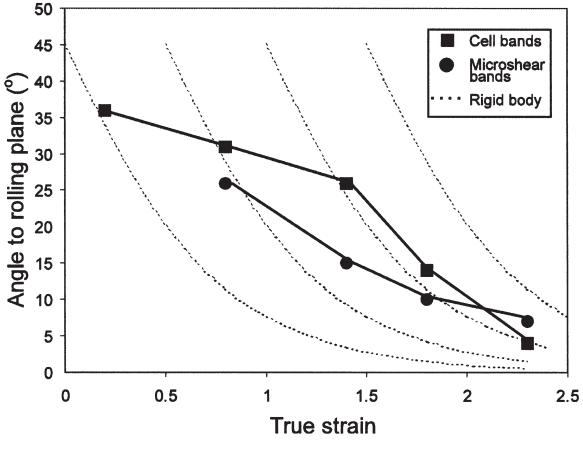

Fig. 2.13. The effect of strain on the alignment of cell and microshear bands with the rolling plane in rolled Al-0.1%Mg. Rigid body rotations are shown for comparison, (after Hurley and Humphreys 2003).

Much of the early work on the characterisation of deformed microstructures was carried out on copper and iron, whereas the extensive work of recent years has concentrated on aluminium and nickel. As discussed above, rather similar features have been identified in all these materials, but detailed and quantitative comparisons between these materials have not yet been made.

2.4.3 Non-cell-forming metals

The addition of 3–5% of magnesium to aluminium in solid solution, hinders dynamic recovery and prevents the formation of dislocation cell structures and many of the other dislocation boundaries discussed in the previous section (Korbel et al. 1986, Hughes 1993, Drury and Humphreys 1996, Kuhlmann-Wilsdorf 2000). Many of the dislocations were found to be arranged in a diffuse geometric pattern along {111} slip planes that defined a so-called **Taylor lattice** (Kuhlmann-Wilsdorf 1989). Adjacent Taylor lattice regions were misoriented by 0.5–1°, and separated by diffuse boundaries **(domain boundaries).** Crystallographically associated microbands, rather similar to those found in copper (fig. 2.11a) were found to develop from these on {111} planes (Korbel et al. 1986, Hughes 1993). As the strain increases, the microbands broaden and cross grain boundaries to become shear bands.

2.5 CUBIC METALS WHICH DEFORM BY SLIP AND TWINNING

In materials with low values of stacking fault energy (silver, austenitic stainless steels, many copper-rich alloys, etc.) a dislocation cell structure does not form and the dislocations dissociate to form planar arrays of stacking faults on the slip planes (fig. 2.14a). At a comparatively early stage of deformation, thin bands of very fine deformation twins then develop.

2.5.1 Deformation twinning

Twinning is a major deformation mode in fcc metals with $\gamma_{SFE} < 25$ mJm^{-2} and in all cph metals. It may also occur in fcc metals with high values of γ_{SFE} and in bcc metals if deformation occurs at low temperatures or high strain rates. In all cases the extent of twinning is orientation dependent.

Manifestations of twinning can be seen on polished surfaces, in etched specimens and in the electron microscope. The well known **strain markings** (fig. 2.14b) have been shown by Duggan et al. (1978b) to consist of very fine deformation twins (fig. 2.14c). These features develop freely on the {111} planes of many fcc alloys of copper and in 18:8 stainless steel. In 70:30 brass, the strain markings appear first near the grain boundaries and in compressed specimens are present on more than one system at strains less than 0.1 (Samuels 1954). They are profuse in most grains at $\varepsilon \sim 0.8$. The width of the markings is determined primarily by γ_{SFE} and the deformation temperature (Hatherly 1959) and as these increase, the markings and the constituent twins become wider (cf. figs. 2.14b and 2.15a). Because of these factors, twinning is a prominent feature of the microstructure of copper after deformation at low temperatures (fig. 2.15b).

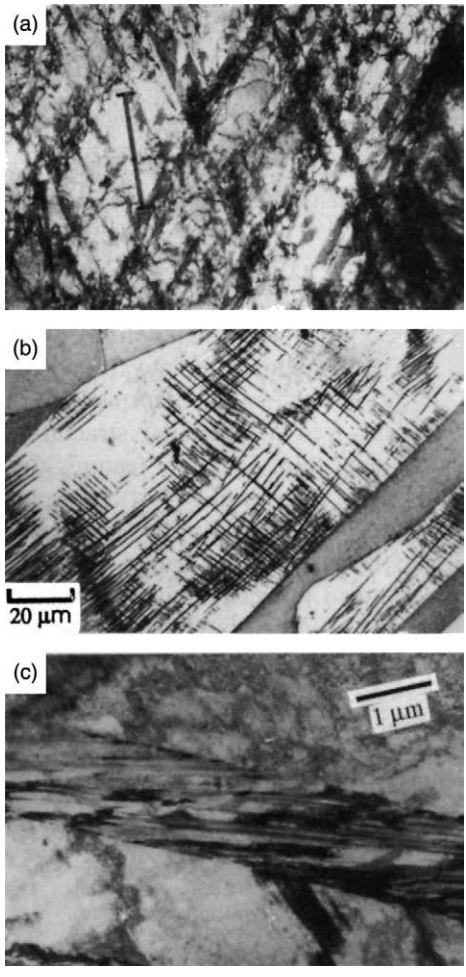

Fig. 2.14. (a) Stacking faults in 15% cold rolled, copper-13at.% aluminium alloy, (Malin 1978), (b) Strain markings in 70:30 brass after 14% compression, (c) deformation twins in 30% cold rolled 70:30 brass, (Duggan et al. 1978b). (All electron micrographs are taken from RD-ND sections, and show 1 μm marker parallel to RD.)

The significance of γ_{SFE} in determining the deformation mode and therefore the nature of the microstructure is apparent in the electron microscope (Duggan et al. 1978b, Wakefield and Hatherly 1981). In low γ_{SFE} materials, the dislocations are dissociated into partials and planar arrays of stacking faults occur (fig. 2.14a). As the strain increases the dislocation content of the faulted structure rises rapidly and bands of very fine twins appear. The size of the twins and their frequency depend particularly on γ_{SFE} and in the following discussion the values given apply to rolled 70:30 brass. The first

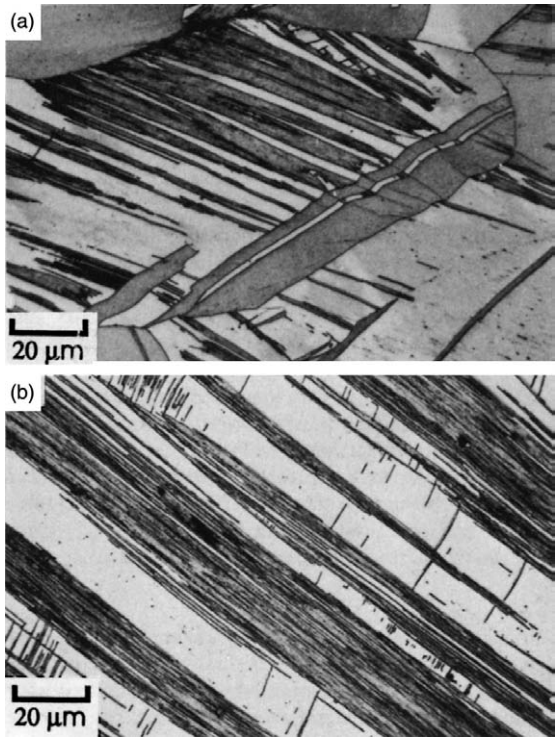

Fig. 2.15. Strain markings in deformed copper and brass showing effects of stacking fault energy and deformation temperature: (a) 90:10 brass compressed 32% at room temperature; (b) (100)[001] single crystal of copper, rolled 60% at −196°C, (Hatherly and Malin 1979).

twins appear at $\varepsilon \sim 0.05$ and clustering into bands follows almost immediately. The twins are extremely fine, with thickness in the range 0.2–0.3 nm, and the twin-parent repeat distance within the bands ranges from 0.5 to 3 nm. These dimensions do not appear to change during deformation but the volume of twinned material increases gradually to about 25%. As rolling proceeds the twins are rotated, as rigid body features, into alignment with the rolling plane and in some grains and deformation bands this process is complete at $\varepsilon \sim 0.8$–1.0 (fig 2.16). The overall twin aligning process continues with further strain and is almost perfect at $\varepsilon \sim 2$.

2.5.2 The effect of stacking fault energy

The effect of stacking fault energy on these structures is very marked. In the very low γ_{SFE} (~ 3 mJm^{-2}) alloy Cu–8.8at% Si, Malin et al. (1982a) reported faulting and twinning on all four {111} planes during rolling to $\varepsilon = 0.4$ (fig. 2.17). In such a structure the gradual alignment of a set of deformation twins with the rolling plane is clearly impossible and in the absence of an alternative deformation mode, shear band

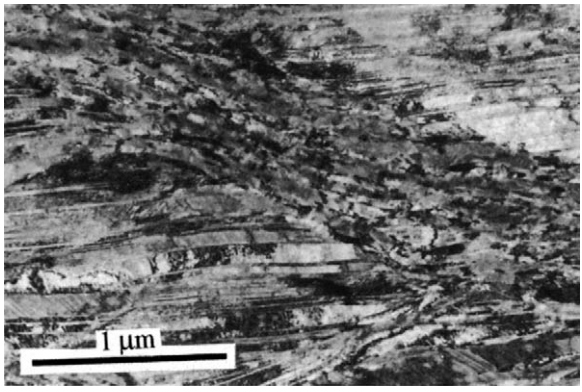

Fig. 2.16. Aligned deformation twins in 50% cold rolled 70:30 brass and inclined shear band, (Duggan et al. 1978b). TD-plane section, (1 μm marker parallel to RD).

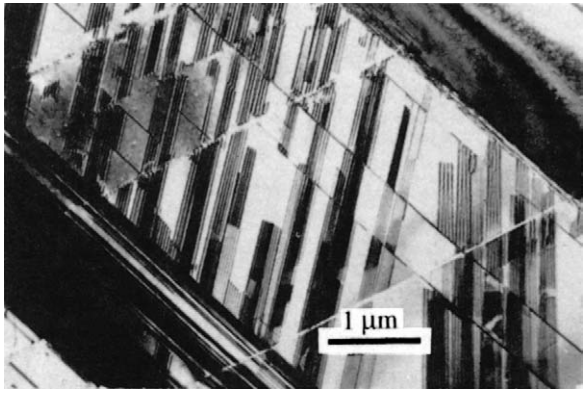

Fig. 2.17. Stacking faults and fine deformation twins in rolled copper-8.8at.%Si, (Hatherly and Malin 1979). TD plane section, (1 μm marker parallel to RD).

formation begins at $\varepsilon = 0.4$–0.5. This alloy cracks along macroscopic shear bands at quite low strains ($\varepsilon \sim 1.2$). In alloys with intermediate values of γ_{SFE}, e.g. 90:10 brass and some stainless steels, the microstructure is determined additionally by the local orientation (Wakefield and Hatherly 1981). In some grains (or deformation bands) the orientation favours twinning and in others slip. The resulting microstructure consists of volumes containing cells and microbands adjacent to volumes showing deformation twins. In some grains where the orientation is appropriate, both slip and twinning occur and as the orientation changes so too does the deformation mode. Twinning is the preferred deformation mode during rolling in regions oriented at $\{112\}<111>$ and $\{100\}<001>$ but twinning is not observed in regions oriented at $\{110\}<001>$ or $\{110\}<112>$. For a discussion of the relationship between orientation and twinning in fcc metals see Köhlhoff et al. (1988a).

2.6 CLOSE PACKED HEXAGONAL (CPH) METALS

As with other metals the deformation of polycrystalline cph metals begins with slip, but the symmetry of the lattice and the availability of slip systems are less than with cubic metals. Under these conditions slip cannot continue as the only deformation mode and twinning becomes significant at quite low strains ($\varepsilon < 0.2$). The most obvious feature of the microstructure of deformed cph metals is the rapid development of a profuse array of large, broad, lenticular deformation twins (fig. 2.18). The twins originate usually as long, thin lamellae at low strain levels, but broaden rapidly. Twins are broader in cph metals than in cubic metals because of the smaller value of the twinning shear. Despite their profusion in the microstructure the contribution of twinning to the overall deformation at medium to high strain levels is usually small. The reason for this lies in the limited magnitude of the twinning shear. As twinning ceases, deformation by slip occurs in the newly developed twins and the whole process is repeated. Tables 2.5 and 2.6 give details of the crystallography of the most frequent slip and twinning systems in cph metals.

Unlike slip, twinning occurs in only one direction, and the crystallography is such that elongation is generated in one direction and contraction in others. Inspection of table 2.6 shows that one twinning system is common to all of the cph metals, viz. $\{10\bar{1}2\} < \bar{1}011 >$. If the c/a ratio is >1.633 (the ideal value), as in zinc and cadmium, twinning occurs only on this system but if c/a is <1.633 more than one system may operate. The strain produced by the twinning shear depends on the twinning system and the value of c/a. For $\{10\bar{1}2\} < \bar{1}011 >$ twinning the strain is greatest for low values of c/a but if other twinning systems are possible these will lead to larger strains. The sense of the shape change also depends on the perfection of packing. For the value $c/a = \sqrt{3} = 1.732$ no twinning is possible but for $c/a < 1.733$ the sense of the shape

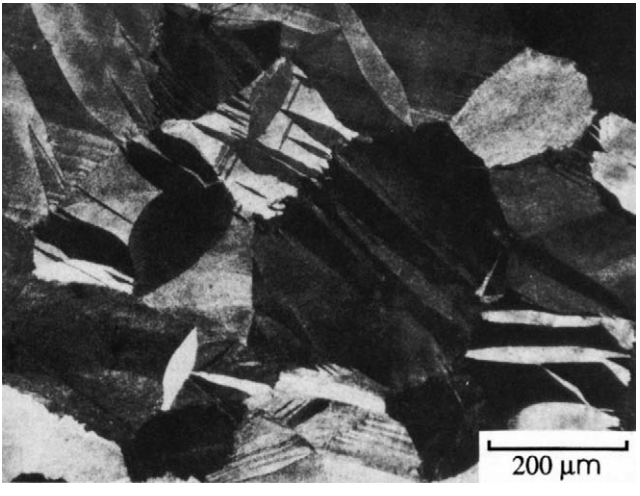

Fig. 2.18. Deformation twins in polycrystalline magnesium deformed 8% in compression at 260°C, (Ion et al. 1982).

Table 2.5
Slip systems in cph metals at room temperature, (Grewen 1973).

Metal	c/a	Slip system	
		Predominant	Seldom
Cd	1.89	$\{0001\} < 11\bar{2}0 >$	$\{11\bar{2}2\} < 11\bar{2}3 >$
Zn	1.88		
Co, Mg	1.62	$\{0001\} < 11\bar{2}0 >$	$\{10\bar{1}0\} < 11\bar{2}0 >$
Zr	1.59	$\{0001\} < 11\bar{2}0 >$	$\{10\bar{1}0\} < 11\bar{2}0 >$
Ti	1.59	$\{10\bar{1}0\} < 11\bar{2}0 >$	$\{0001\} < 11\bar{2}0 >$

Table 2.6
Twinning systems in cph metals, (Grewen 1973).

Metal	c/a	Twinning shear	Twinning element	
			Plane	Direction
Cd	1.89	0.17		
Zn	1.88	0.14	$\{10\bar{1}2\}$	$< \bar{1}011 >$
Co	1.62	0.13		
Mg	1.62	0.13	$\{10\bar{1}2\}$	$< \bar{1}011 >$
Zr,Ti	1.59	0.167	$\{10\bar{1}2\}$	$< \bar{1}011 >$

change is opposite to that for $c/a > 1.732$. In practice this means that twinning should occur only if directions that are shortened by twinning lie in the appropriate directions during processing, e.g. radially during wire drawing.

It will be seen that for metals with c/a greater than ideal, basal slip is favoured while prismatic slip is preferred for those with c/a less than ideal. In general dislocations are confined to the closely packed basal plane and do not move freely from it. There have been only a few detailed examinations of the deformation microstructure in any of these metals and it is difficult to draw general conclusions.

In rolled titanium (c/a < ideal) deformation twinning is found in all grains at a very early stage (Blicharski et al. 1979). The twins are broad and lenticular and usually form on two or more systems. Because of the small twinning shear, further deformation requires the formation of smaller twins between and within those first formed, but eventually this is no longer possible and fresh twins do not form at moderate strain levels ($\varepsilon \sim 0.75$). At high strain levels the twins undergo a rigid body rotation into alignment with the rolling plane so as to produce a microstructure of thin elongated bands. Shear bands begin to

form at $\varepsilon \sim 2.8$ in this aligned structure but considerable ductility still remains at much higher strain levels.

The microstructure of deformed zinc is interesting. The c/a ratio is high and so too is γ_{SFE} ($\sim$140 mJm^{-2}), but the melting point is low and room temperature deformation occurs at $\sim 0.4T_m$. Large twins are seen in every grain of polycrystalline zinc after very light rolling ($\varepsilon = 0.07$) but no further twins develop as rolling continues to $\varepsilon = 0.2$ and slip is the preferred deformation mode in this strain range (Malin et al. 1982b). Shear band formation begins in the strain range $0.2 < \varepsilon < 0.5$ but the shear bands are detected only by the presence of bands of very small recrystallized grains that outline their positions. It seems clear that recrystallization follows shearing closely in this low melting point metal. The new strain-free grains deform by slip and twinning and deformation continues in this way to high strain levels. These changes are easily recognized in the deformation textures and will be referred to in chapter 3.

2.7 DEFORMATION BANDS

As discussed in §2.4.1 and shown in figures 2.8 and 2.9c and 2.9d, the coarsest form of grain subdivision is the formation of deformation bands, and because these are easily identified by optical microscopy, they have been recognized for a long time. Major attention was first focused on them by Barrett (1939) who argued that inhomogeneities of this type contributed to the inability to predict the strain hardening behaviour and the orientation changes taking place during deformation. Following Barrett the term **deformation band** is used to describe a volume of approximately constant orientation, that is significantly different to the orientation(s) present elsewhere in that grain. Kuhlmann-Wilsdorf et al. (1999) have presented an extensive review of the early work on deformation bands and on the conditions under which they form.

2.7.1 The nature of deformation bands

The different features are illustrated schematically in figure 2.8c which shows a region B, which has a different orientation to that in the grain proper A. The region at the edge of the deformation band where the orientation changes from B to A may have a finite width, in which case it is called a **transition band.** However, in some cases the orientation change is sharp, and this is then a **deformation-induced grain boundary.** In many cases deformation bands occur with approximately parallel sides and involve a double orientation change A to C and then C to A. A deformation band of this special type is called a **kink band** following the nomenclature of Orowan (1942). The micrograph of figure 2.9c shows a complex microstructure of kink bands and deformation bands in α-brass, and figure 2.9d shows deformation bands in an Al–Mg alloy. The development of deformation bands is an inevitable consequence of the deformation of polycrystals (and also of constrained single crystals), and the details of the microstructure are determined by the crystallographic nature of the deformation process.

2.7.2 The formation of deformation bands

The nature and formation of deformation banding has been extensively studied in recent years because of its relevance to the generation of deformation textures. Chin (1969) identified two types of deformation bands. One of these originates in the ambiguity associated with the selection of the operative slip systems. In many cases the imposed strain can be accommodated by more than one set of slip systems and the different sets lead to rotations in different senses. In the second type, different regions of a grain may experience different strains if the work done within the bands is less than that required for homogeneous deformation and if the bands can be arranged so that the net strain matches the overall deformation. This latter is similar to the reasoning used to explain the formation of cell blocks (§2.4.1). In their model of rolling texture development, Lee et al. (1993) examined the second of these cases and showed theoretically that as few as two independent slip systems may suffice to accommodate the shape change. Their work is consistent with the relaxed constraints models of plasticity discussed in §3.7.1. Kuhlmann–Wilsdorf (1999) has recently discussed the formation of deformation bands in terms of her low energy dislocation model.

2.7.3 Transition bands

A transition band develops when neighbouring volumes of a grain deform on different slip systems and rotate to different end orientations. In its most usual form the transition band consists of a cluster of long narrow cells or subgrains with a cumulative misorientation from one side of the cluster to the other. It is sometimes found, particularly in aluminium alloys (Hjelen et al. 1991), that the width of the transition band is reduced to only one or two units but the large orientation change across the band is retained.

Dillamore and Katoh (1974) considered the case of axisymmetric compression of iron and showed that the rotation paths for various orientations followed those shown in figure 2.19a. For orientation gradients that straddle the line joining [110] and [411] a very sharp transition band develops as part of the gradient rotates towards [100] and part towards [111]. The more general case is shown at A. For the gradient B–B′ both extremities rotate towards [111] and the heterogeneity is gradually lost. For a gradient C–C′ the extremes follow different paths and misorientation persists in a diminished form. Figure 2.19b shows that the experimentally determined fibre texture after 88% compression is in good agreement with the model used. Dillamore and Katoh also considered the special case of the formation of a transition band in heavily rolled copper having the orientation $\{100\}<001>$ at its centre. The implications of the Dillamore–Katoh model for the generation of the cube texture during recrystallization are discussed in chapter 12.

2.7.4 The conditions under which deformation bands form

The details of transition band formation depend strongly on the grain orientation, as discussed above. However, the occurrence of deformation bands is dependent on the microstructure and deformation conditions.

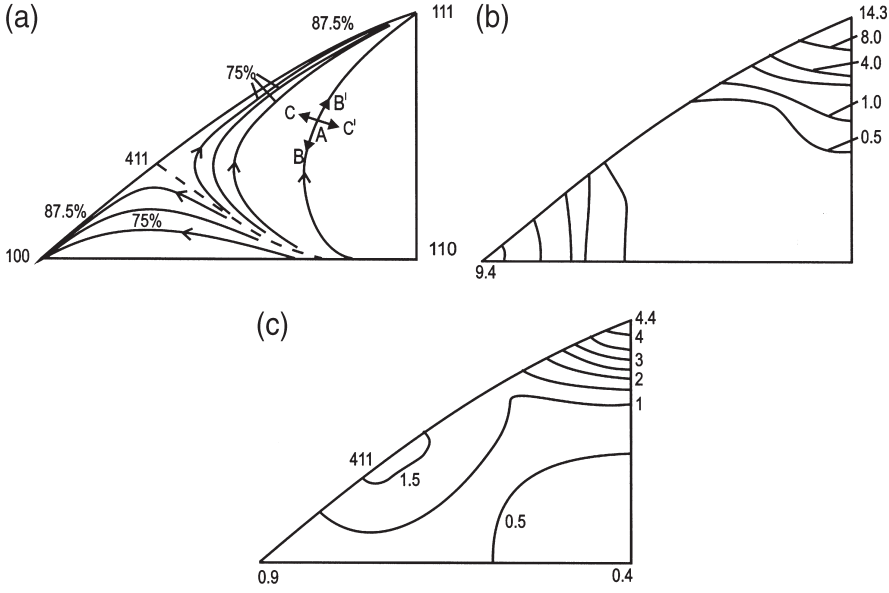

Fig. 2.19. Texture development in axially compressed iron. (a) Predicted rotations from three different initial orientations after 70% and 88% reduction in thickness, (b) Deformation texture after 88% compression, (c) Recrystallization texture of (b) material, (after Dillamore et al. 1974).

The **grain orientation** is an important factor in determining whether or not a grain will deform relatively homogeneously or fragment by deformation banding, as may be seen from figure 2.19. For example, the $\{110\}<001>$ Goss orientation in fcc materials is very stable under condition of plane strain deformation (§3.7.1.4), and single crystals (Ferry and Humphreys 1996a), and large-grained polycrystals (Somerday and Humphreys 2003b) can undergo extensive deformation without the development of large-scale heterogeneities, as seen in figure 7.15.

The **initial grain size** is of particular importance, and deformation banding occurs much more readily in coarse grained metals, as reviewed by e.g. Kuhlmann–Wilsdorf (1999), Humphreys et al. (1999). Lee and Duggan (1993) measured a decrease in the numbers of deformation bands per grain in copper with decreasing grain size, and Humphreys et al. (1999) concluded that in aluminium, deformation banding did not occur in material with a grain size less than $\sim$20 μm. Lee et al. (1993) using an energy criterion, predicted that the number of deformation bands per grain should be proportional to the square root of the grain size.

There is extensive evidence that deformation banding **decreases at higher temperatures** (see e.g. Kuhlmann–Wilsdorf et al. 1999). This effect is discussed in §13.2, and may be seen in figure 13.6.

2.8 SHEAR BANDS

Shear bands, which occur in many metals and alloys, were described in detail by Adcock (1922), but until the work of Brown (1972) on aluminium and Mathur and Backofen (1973) on iron, were largely forgotten. These bands correspond to narrow regions of intense shear that occur independently of the grain structure and independently also of normal crystallographic considerations. In rolled material they occur at $\sim 35^\circ$ to the rolling plane and parallel to the transverse direction (figures 2.8d, 2.9e and 2.9f). Note the offsets at the scratch in figure 2.9e which show the shear associated with the bands.

2.8.1 Metals of medium or high stacking fault energy

At high strain levels, $\varepsilon > 1.2$ for copper, shear bands form in colonies in each of which only one set of parallel bands develops (fig. 2.9e). The colonies are usually several grains thick and the bands in alternate colonies are in opposite senses, so that a herringbone pattern develops (Malin and Hatherly 1979). Any grain boundaries in the colony are crossed without deviation. The structure of a shear band is clearly resolved in figure 2.20a; the aligned microbands of the rolled iron have been swept into the shear band and local elongation and thinning have contributed to the shear strain. The distinct lattice curvature of figure 2.20a is characteristic of a shear band that has been associated with only light to moderate shearing, and the similarity to the microshear (S) bands in deformed aluminium (figure 2.12a) can be seen. A typical microstructure formed at large strains is shown in figure 2.20b. The shear in bands of this type is large, and values as high as 6 have been reported, although 2–3 is a more usual value. At still higher levels of strain, larger shear bands develop which cross a rolled sheet from one surface to the other and when eventually a uniform population of these bands exists, failure occurs along them.

2.8.2 Metals of low stacking fault energy

The shear band morphology in materials with low values of γ_{SFE} is quite different to that found in metals which do not develop deformation twins (Hatherly 1982, Hatherly and Malin 1984). In rolled 70:30 brass, isolated shear bands are first seen at $\varepsilon \sim 0.8$ and specifically in regions where twin alignment with the rolling plane is already well established (fig. 2.16; Duggan et al. 1978b), and soon afterwards ($\varepsilon \sim 1$) two families of shear bands are seen in many regions. The bands form initially at approximately $\pm 35^\circ$ to the rolling plane and divide the sheet into rhomboidal prisms with long axes parallel to TD. The twin alignment within the prisms is nearly perfect and most theories of shear band formation are based on the supposition that continued deformation by either slip or twinning is no longer viable in such an aligned structure. As shown in figure 2.21, the bands themselves consist of an array of very small 'crystallites' (volumes of almost perfect lattice) which are usually elongated in the direction of shear with aspect ratios in the range of 2:1–3:1. Typical shear bands in 70:30 brass range in thickness from 0.1–1 μm and the individual crystallites vary in width from 0.02–0.1 μm.

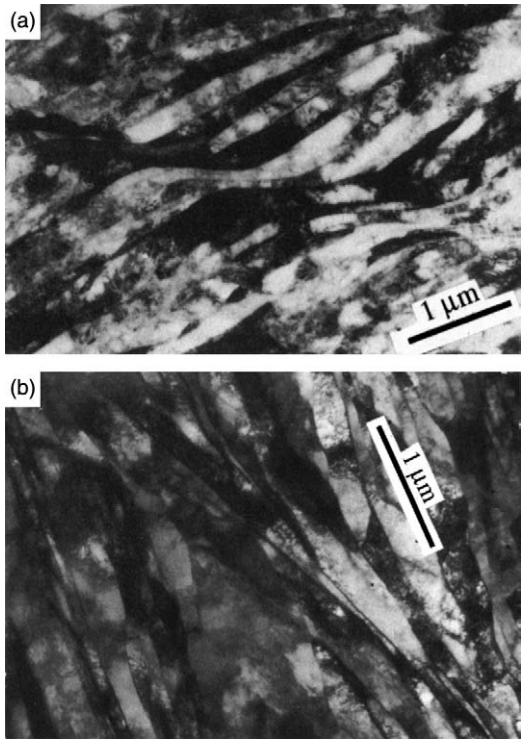

Fig. 2.20. Shear bands in metals deforming by slip. (a) Shear band in 85% cold rolled iron (Willis 1982). (b) Shear band in 97% cold rolled copper, (Malin and Hatherly 1979). (ND-RD plane; 1 μm marker parallel to RD).

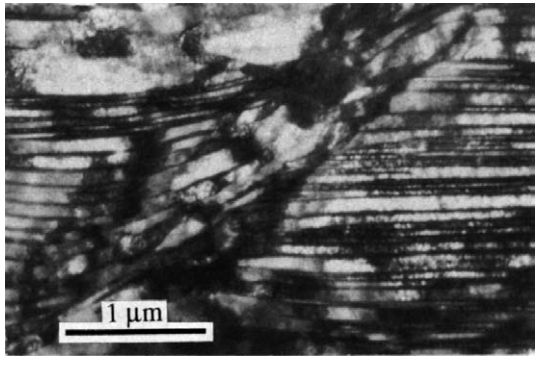

Fig. 2.21. Internal crystallite structure in a shear band in a (110)[111] copper single crystal, cold rolled 65% at 77°K, which has deformed by twinning, (Köhlhoff et al. 1988a). (ND-RD section with 1 μm marker parallel to RD).

The orientations of the crystallites are particularly interesting. Their volume in heavily deformed metals is such that they should make a significant contribution to the rolling texture, and shear bands are a major nucleation site for recrystallized grains. Duggan et al. (1978a) reported large ($>20^\circ$) orientation differences between neighbouring crystallites in 70:30 brass that were not cumulative. An overall preference was detected for rolling plane orientations near {110} and a substantial population was found near $\{110\}<001>$. This orientation is a major component of the shear texture in fcc metals.

The shear associated with individual bands is high with average values of 3–4 often reported but shears as high as 10 are sometimes found (Duggan et al. 1978b). The importance of shear band formation as a deformation process is strikingly illustrated by figure 2.22. A longitudinal section from a specimen of 50% cold rolled, 70:30 brass, was polished and then lightly scratched at right angles to the rolling direction. The figure shows the development of shear bands during a subsequent rolling of 10% reduction and the magnitude of the shear strain. The number of shear bands increases rapidly with strain and in the range $0.8 < \varepsilon < 2.6$ shear band formation appears to be the major deformation mode and at the latter level of strain only minor amounts of twinned material remain. As in the case of high γ_{SFE} materials, further deformation leads to the formation of large through-thickness shear bands and eventually fracture occurs along these.

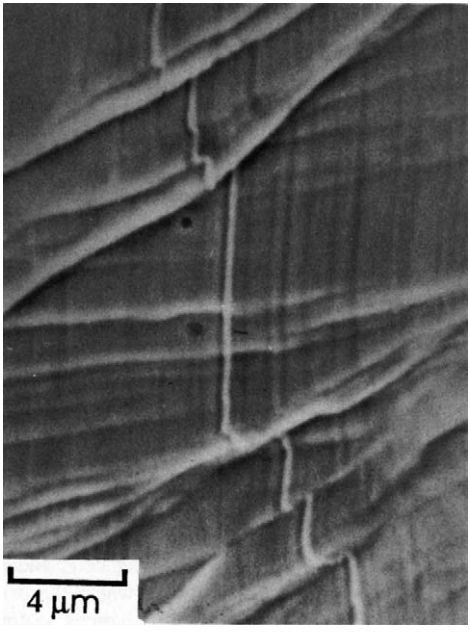

Fig. 2.22. 70:30 Brass specimen initially rolled 50%, then polished and lightly scratched normal to rolling direction before further rolling of 10% reduction (TD-plane section). Note the magnitude of the shear, (Duggan et al. 1978b).

2.8.3 The formation of shear bands

A shear band is a form of plastic instability and in plane strain deformation (or rolling) the condition for instability is

$$\frac{1}{\sigma}\frac{d\sigma}{d\varepsilon} < 0 \tag{2.9}$$

Dillamore and colleagues (Dillamore 1978a, Dillamore et al. 1979), have written this condition as

$$\frac{1}{\sigma}\frac{d\sigma}{d\varepsilon} = \frac{n}{\varepsilon} + \frac{m}{\dot{\varepsilon}} + \frac{1+n+m}{M_T}\frac{dM_T}{d\varepsilon} - \frac{m}{\rho}\frac{d\sigma}{d\varepsilon} < 0 \tag{2.10}$$

where n and m are the usual strain hardening and strain rate exponents, ρ the dislocation density, and M_T the Taylor factor (defined as Σ_S/ε, where Σ_S is the total shear strain on all active slip systems, and ε is the normal strain).

Of the various terms in the equation, that in ε is always positive, that in $\dot{\varepsilon}$ is usually positive and that ρ is negative. It follows that if instability is to occur at medium to high strain levels, and in the absence of strain rate effects, it must be because the term in M_T becomes negative through a negative value of $dM_T/d\varepsilon$. This latter expression corresponds to geometric softening, in that instability is favoured if it causes a lattice rotation into a geometrically softer condition. $dM_T/d\varepsilon$ can be calculated from $dM_T/d\theta$ (the rate of change of hardness with orientation) and $d\theta/d\varepsilon$ (the rate of change of orientation with strain). Dillamore et al. (1979) have shown that this factor is both negative and a minimum close to $\pm 35^\circ$ for typical rolled metals with well developed textures.

2.8.4 The conditions for shear banding

The 'copper type' shear bands discussed in §2.8.1 occur in a variety of metals, and their occurrence depends on a number of factors.

Grain size – Several authors including Ridha and Hutchinson (1984) and Korbel et al. (1986) have shown that the tendency for shear banding increased with increasing grain size.

Orientation – The effect of orientation on shear banding has been demonstrated by Morii et al. (1985) in single crystals of Al–Mg.

Solute – The addition of manganese to copper, which does not affect the stacking fault energy, leads to the formation of extensive shear banding (Engler 2000) and magnesium promotes shear banding in aluminium (Duckham et al. 2001).

Deformation temperature – Several authors have demonstrated that shear banding becomes less common at high temperatures. The combined effects of deformation temperature and strain on the tendency for shear banding in Al–1%Mg are well summarised in figure 2.23 from the work of Duckham et al. (2001).

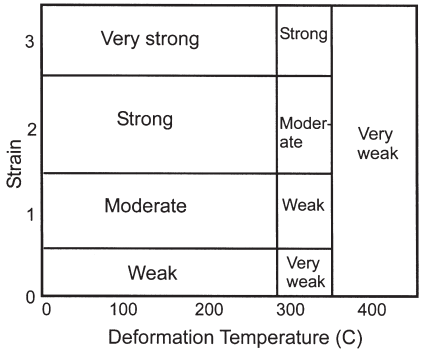

Fig. 2.23. The tendency for shear band formation in Al–1%Mg as a function of strain and deformation temperature, (Duckham et al. 2001).

2.9 THE MICROSTRUCTURES OF DEFORMED TWO-PHASE ALLOYS

Most industrial alloys contain more than one phase, the microstructure comprising a matrix phase and dispersed second-phase particles. If these particles are present during deformation, they will affect the microstructure, and this in turn may affect the subsequent annealing behaviour. The most important aspects of the deformation structures in two-phase alloys in this respect are:

- **The effect of the particles on the overall dislocation density.** This may increase the driving pressure for recrystallization.
- **The effect of the particles on the inhomogeneity of deformation in the matrix.** This may affect the availability and viability of the sites for recrystallization.
- **The nature of the deformation structure in the vicinity of the particles.** This determines whether or not particle-stimulated nucleation of recrystallization (PSN) will be possible.

During deformation of an alloy containing second-phase particles, the dislocations will bow around the particles as shown in figure 2.24. An analysis of the situation in terms of elementary dislocation theory follows. For particles of radius r and spacing λ along the dislocation line, the force exerted on each particle (F) is given by:

$$F = \tau b \lambda \tag{2.11}$$

where τ is the applied stress.

If the strength of the particle is less than F, then the particle deforms, otherwise the dislocation reaches the semicircular configuration of figure 2.24b, when the applied stress is given by

$$\tau_0 = \frac{Gb}{\lambda} \tag{2.12}$$

which is the well known **Orowan stress.**

The dislocation then proceeds to encircle the particle, leaving an **Orowan loop** as shown in figure 2.24c. A micrograph of such loops in a nickel alloy is shown in figure 2.25. Because of its line tension, an Orowan loop exerts a shear stress on the particle which is given approximately by

$$\tau = \frac{Gb}{2r} \tag{2.13}$$

If the particle is strong enough to withstand this stress, it does not deform and the net result of the passage of a matrix dislocation is the generation of extra dislocation in the

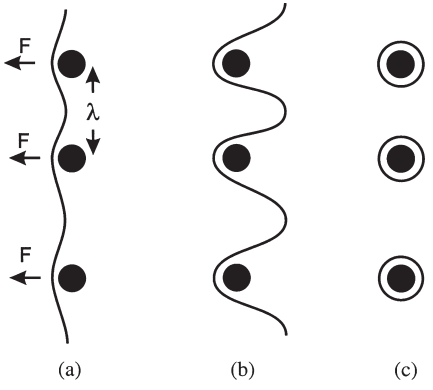

Fig. 2.24. The formation of Orowan loops at second-phase particles.

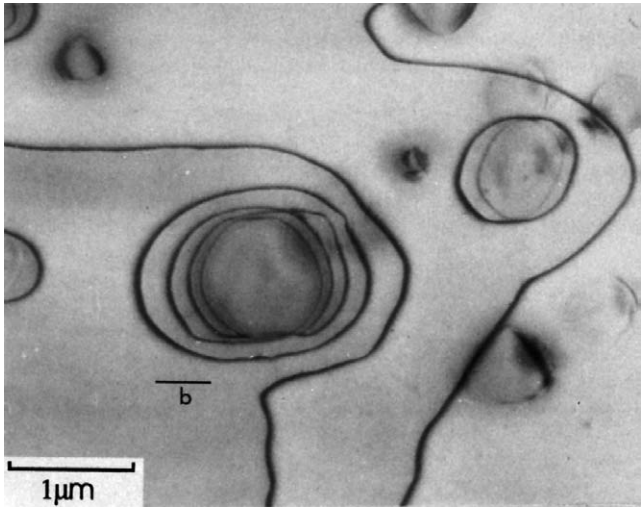

Fig. 2.25. Orowan loops at Ni_3Si particles in a Ni–6%Si single crystal, (Humphreys and Ramaswami 1973).

form of the Orowan loop, at the particle. If the particle deforms either before or after the Orowan configuration is reached, no extra dislocations are generated at the particle.

Detailed discussion of the factors affecting the strength of particles is beyond the scope of this volume, and the reader is referred to the reviews of Martin (1980), Brown (1985), Humphreys (1985) and Ardell (1985) for further details. However it is important to realise that the subsequent deformation behaviour and hence **the density and arrangement of dislocations in the deformed material is dependent on whether or not the particles deform.**

2.9.1 Dislocation distribution in alloys containing deformable particles

If the particle of figure 2.26a deforms as shown in figure 2.26b, then its size on the slip plane is effectively reduced by the Burgers vector b of the dislocation. As a smaller particle is normally weaker than a larger particle, the slip plane is softened and subsequent dislocations will tend to move on the same plane, thus concentrating slip into bands as shown in figure 2.26d. This is illustrated in the micrograph of figure 2.27, where shear offsets of ~0.1 μm indicate the passage of several hundred dislocations on the same plane.

The slip distribution in alloys containing small particles has been discussed by Hornbogen and Lütjering (1975) and by Martin (1980) as follows.

The yield stress of a crystal containing deformable particles is often given by an equation of the form

$$\tau = CF_V^{1/2}d^{1/2} \tag{2.14}$$

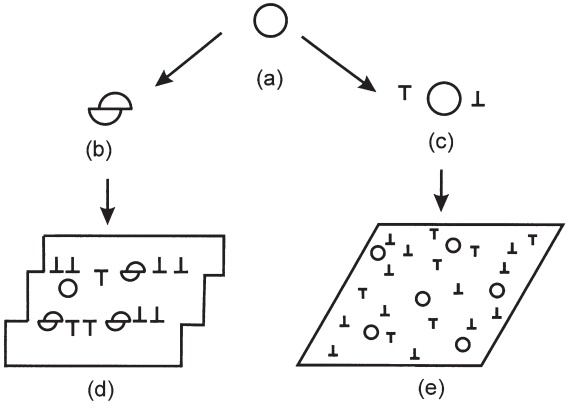

Fig. 2.26. The effect of particle strength on the distribution of slip. A deforming particle (b) leads to slip concentration (d). A non-deforming particle (c) results in more homogeneous slip (e).

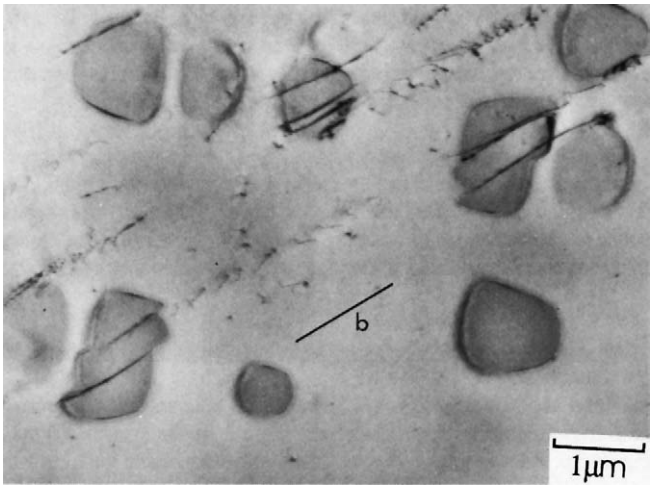

Fig. 2.27. Deformed Ni_3Si particles in a Ni–6%Si single crystal, (Humphreys and Ramaswami 1973).

where C is a constant dependent upon the particular hardening mechanism which is operative (e.g. coherency strains). If n dislocations shear a particle, the diameter of the particle will be reduced by nb. The stress for further deformation then becomes

$$\tau = C F_V^{1/2}(d - nb)^{1/2} = C F_V^{1/2} d^{1/2} \left(1 - \frac{nb}{d}\right)^{1/2} \tag{2.15}$$

Thus the slip plane is softened, so that further slip tends to occur on that plane. This is in contrast to the case of non-deformable particles, where the dislocation debris left by previous dislocations (e.g. the Orowan loops of fig. 2.25) makes it more difficult for slip to occur on the same plane, thus tending to make slip relatively homogeneous (fig. 2.26e).

The amount by which a slip plane is weakened by the passage of a dislocation is the parameter $d\tau/dn$, and differentiation of equation 2.15 gives

$$\frac{d\tau}{dn} = \frac{-bCF_V^{1/2}}{2d^{1/2}} \left(1 - \frac{nb}{d}\right)^{-1/2} \tag{2.16}$$

We thus see that the tendency for coarse slip is increased by small particles, a large volume fraction and a large value of C.

There are many recorded examples of particle shearing leading to slip concentration. This is of particular concern in the design of high strength precipitation hardened alloys, in which the slip concentration may adversely affect the fracture toughness and the fatigue behaviour (e.g. Polmear 1995). An example of this is found in binary Al–Li alloys

in which precipitates of the ordered δ' phase are formed. These particles deform during deformation, leading to extensive shear localisation (Sanders and Starke 1982).

As the shape and size of the particles changes during deformation, so the slip distribution may also be a function of strain. Kamma and Hornbogen (1976) found that small platelike particles of Fe_3C in steel deformed, leading to the formation of shear bands. However, at high strains, the bands broadened, and the slip became homogeneous. Nourbakhsh and Nutting (1980) showed that in overaged Al–Cu alloys containing large plates of θ', the deformation was initially inhomogeneous as the θ' plates deformed. At strains above 1, the plates disintegrated to give small spherical particles and as found by Kamma and Hornbogen, a more homogeneous slip distribution resulted. The same authors also found that in the underaged alloy, the small GP zones which resulted in slip concentration at lower strains, were dissolved at strains of 5 and the deformation behaviour of the alloy then became similar to that of the solid solution.

We therefore conclude that the slip distribution in alloys containing deformable particles is complex and may alter with strain as changes in the particle size and shape are induced by the deformation.

2.9.2 Dislocation distribution in alloys containing non-deformable particles

2.9.2.1 Dislocation density

If a deforming matrix contains non-deformable particles, then, as was first shown by Ashby (1966, 1970) there is a strain incompatibility between the two phases as shown in figure 2.28. In figure 2.28a, a spherical particle of radius r is contained within an undeformed matrix. On deformation by a shear strain s, then, as shown in figure 2.28b, a deformable particle will comply with the imposed strain. However, if the particle does not deform, then as shown in figure 2.28c, there is a local strain incompatibility. This can be accommodated by the generation of dislocations at the particle-matrix interface and also, if the interface is weak, by the formation of voids. A more detailed consideration of the dislocation generation near the particle is given in §2.9.3. However, the length of dislocation generated is not very sensitive to the details of the mechanism, and it is readily shown that the incompatibility may be accommodated approximately by the generation of n circular prismatic dislocation loops of Burgers vector b and radius r, where

$$s = \frac{nb}{2r} \tag{2.17}$$

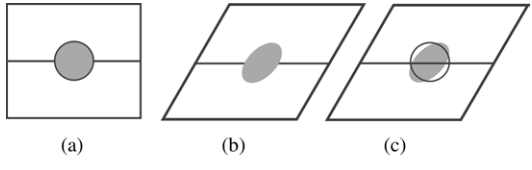

Fig. 2.28. The incompatibility between a deforming matrix and a non-deforming particle. (a) undeformed, (b) deformed particle, (c) non-deformable particle.

The length of dislocation per particle, L, is thus

$$L = \frac{4\pi r^2 s}{b} \tag{2.18}$$

and the dislocation density (ρ_G) due to this effect is $N_V L$. Taking N_V as given by equation A2.11, then

$$\rho_G = \frac{3F_V s}{rb} \tag{2.19}$$

These have been termed the **geometrically necessary** dislocations by Ashby.

The total density of dislocations generated in the material will be approximately $\rho_G + \rho_s$, where ρ_s is the density of dislocations which would be generated in the single-phase matrix (see §2.2). However, because dislocations will be lost by recovery during or after the deformation, this is an upper limit. Figure 2.29 shows the estimated density of dislocations ($\rho_G + \rho_s$) generated for a matrix of grain size 100 μm (equations 2.1 and 2.19), as a function of strain and particle content, neglecting the effects of dynamic recovery.

Although there is little quantitative data, there is evidence that in particle-containing single crystals or polycrystals deformed to **small strains,** the dislocation density is much greater than in single-phase materials of similar composition. For single crystals of copper, oriented for single slip, and containing alumina particles, Humphreys and Hirsch (1976) found that the dislocation density was close to that predicted by equation 2.19. However, analysis of the data of Lewis and Martin (1963) on copper polycrystals containing oxide particles shows that the dislocation densities at tensile strains of 0.08 are very much lower than those predicted. There is little data available for large strains, where the situation is often complicated by dynamic recovery and the formation of dislocation boundaries rather than free dislocations.

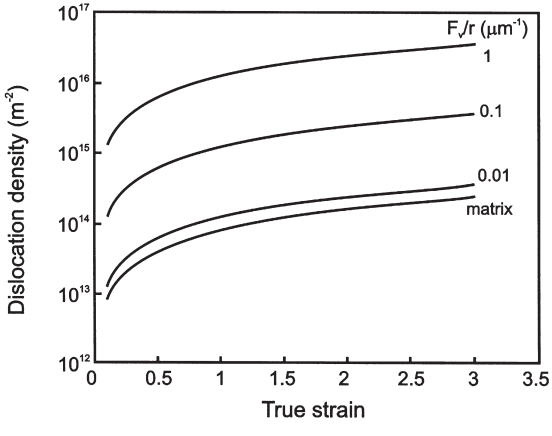

Fig. 2.29. Predicted dislocation densities in particle-containing alloys.

There are comparatively few direct measurements of the stored energy of particle-containing alloys. Adam and Wolfenden (1978) found the stored energy of an Al-Mg-Si alloy deformed to a strain of 0.1 to be some ten times that of pure aluminium. Measurements of stored energy in particle-containing copper alloys by Baker and Martin 1983a (fig. 9.6a), show an increase in stored energy with strain which is in approximate agreement with equation 2.19 at low strains, with some indication that the stored energy saturates at strains larger than $\sim$1. Other measurements of the stored energy of dispersion hardened copper alloys deformed to large strains (Bahk and Ashby 1975, Chin and Grant 1967) indicate that the stored energy in these alloys is not significantly greater than for pure copper.

As the dislocation density is generally found to be directly related to the flow stress (equation 2.2), some indication of the change in dislocation content with strain may often be inferred from the stress-strain behaviour. From such experiments, there is considerable evidence that the work hardening in two-phase alloys, which is initially high, frequently falls to that of a comparable single-phase alloy after strains of $\sim$0.05 in copper (Lewis and Martin 1963), in steels (Anand and Gurland 1976), and in aluminium alloys (Lloyd and Kenny 1980).

In summary, it is apparent that the large increase in dislocation density predicted by equation 2.19 and figure 2.29, for alloys containing small non-deformable particles are only obtained for very small strains, and that at the larger strains which are usually of importance for recrystallizing materials, dynamic recovery may reduce the dislocation density to a value little larger than that for a single-phase alloy.

2.9.2.2 Cell and subgrain structures

It has often been reported that particles affect the dislocation cell structures formed on deformation. As discussed in §2.2.3, cell and subgrain structures are products of dynamic recovery and will therefore be greatly influenced by any parameters which affect the generation or the recovery of dislocations.

A dispersion of small non-deformable second-phase particles results in dislocation generation (§2.9.2.1) and also affects dynamic recovery by impeding the movement of dislocations. Dislocations will only pass strong particles if the local stress exceeds that given by equation 2.12. Therefore although dislocations will be free to move in the regions between particles, they will tend to be held up at particles. In a similar manner, the particles will pin cell or subgrain boundaries (§4.6). Recovery processes which occur on a scale **smaller** than the interparticle spacing (λ) will therefore be relatively unaffected by the particles, but recovery processes involving rearrangement of dislocations on a scale **larger** than the interparticle spacing will be hindered. The interparticle spacing may therefore be expected to affect the size and misorientation of the dislocation cells or subgrains. The cell size (D) is typically 0.5–1 μm in many metals and decreases with increasing strain (fig. 2.4). If $\lambda < D$ we would expect the cell structure to be affected by the particles. However, if $\lambda > D$, the particles would be expected to have little effect on cell formation.

The cell size – Observations of cell formation in dispersion strengthened copper with very small interparticle spacing ($\lambda \sim 0.1$ μm) (Lewis and Martin 1963 and

Brimhall et al. 1966) indicate that compared with copper, the dislocation cells are more diffuse, form at larger strains, and have a size related to the interparticle spacing. However, in oxide-containing aluminium (Hansen and Bay 1972) and copper (Baker and Martin 1983b), where the interparticle spacing is 0.3 to 0.4 μm, the cell size was not found to significantly differ from that of the pure matrix. In a study of the effect of strain on the substructure of two-phase aluminium alloys, Lloyd and Kenny (1980) found that at low strains the cell size was related to the interparticle spacing, but at larger strains, the cell size was reduced and was almost independent of particle size as shown in figure 2.30. Recent EBSD measurements shown in table 2.7 also indicate that the cell sizes in particle-containing and particle-free alloys are similar.

The cell misorientation – Early electron diffraction experiments on copper (e.g. Brimhall et al. 1966) indicated that the lattice misorientation between cells in alloys with a small interparticle spacing, was less than in the single-phase matrix. However, later work on copper (e.g. Baker and Martin 1983b) and aluminium (Hansen and Bay 1972), in which the interparticle spacings were larger, found the misorientations to be similar to those of single-phase alloys.

Results of a recent EBSD investigation of aluminium and copper alloys, both of which have been shown to contain sufficient particles to prevent recrystallization, are shown in table 2.7. For both aluminium and copper, the particles do not significantly affect the cell size. However, in both cases the cell misorientations are greatly reduced by the particles, and it is significant that the **long range orientation gradients,** which were measured as the extreme (uncorrelated) misorientations within a 10 μm x 10 μm area, were also shown to be much smaller in the particle-containing materials. These give general confirmation of the earlier results which showed that **where the interparticle spacing is similar to the cell size, there is a corresponding homogenisation of the deformation microstructure.**

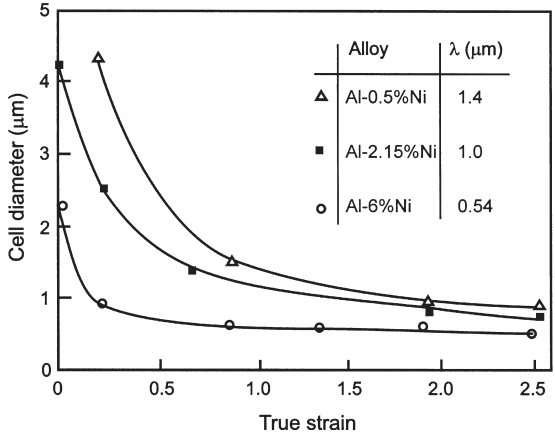

Fig. 2.30. The cell size as a function of strain in Al–Ni alloys, (after Lloyd and Kenny 1980).

Table 2.7
The effects of small, non-deformable, second-phase particles on local and long range misorientations in copper and aluminium, determined by EBSD. (Al–Si samples from Humphreys and Brough (1997), Cu–Al_2O_3 samples from Humphreys and Ardakani (1996)).

Alloy	Particle			Subgrain		Orientation spread (°) in 10×10 μm
	d (μm)	$\mathbf{F_V}$	λ (μm)	Size (μm)	Mis'n (°)	
Al–0.1Mg	—	—	—	0.9	2.1	12
Al–0.8Si	0.10	8×10^{-3}	0.80	1.1	1.4	7
Cu (5n)	—	—	—	0.35	1.5	21
Cu–Al_2O_3	0.05	7×10^{-3}	0.43	0.32	0.9	9

2.9.2.3 Larger scale deformation heterogeneities

There is less evidence as to the effect of non-deformable particles on larger scale heterogeneities in the deformation structure such as **deformation bands** or **shear bands.** During the deformation of single-phase alloys, a grain may, in addition to changing orientation, deform inhomogeneously and divide into regions of different orientation as shown in figures 2.31a and b (cf. fig. 2.8c), and Habiby and Humphreys (1993) found evidence that large (>1 μm) silicon particles could act as nucleation sites for such deformation bands in aluminium. Humphreys and Ardakani (1994) found that during the deformation in plane-strain compression of aluminium crystals of the unstable (001)[110] orientation, the crystal split into two orientations which rotated towards the stable 'copper' orientations (112)[11$\bar{1}$] and ($\bar{1}\bar{1}$2)[111], as shown schematically in figure 2.31b. Large non-deforming particles, by modifying the plastic deformation close to the particle caused a small portion of crystal to rotate in the 'wrong' sense (fig. 2.31c), thus nucleating a small deformation band within one of the components which had the orientation of the other component. Ferry and Humphreys (1996b) found a similar effect in particle-containing crystals of the $\{011\}<100>$ Goss orientation.

It is probable that large inclusions may be responsible for **nucleating** deformation bands by such a mechanism in many commercial alloys. However there is no indication (Habiby and Humphreys 1993) that sub-micron sized particles have any significant effect on the **scale** of deformation band formation in aluminium.

Particles may also affect the formation of **shear bands** which, as discussed in §2.8 are often the result of a low rate of work hardening. This is frequently found for alloys containing deformable second-phase particles (§2.9.1), and a number of investigations have reported the formation of shear bands in such alloys (e.g. Kamma and Hornbogen 1976, Sanders and Starke 1982, Lücke and Engler 1990). In alloys containing large volume fractions of non-deformable particles, the initially high work hardening rate is not maintained to high strains and therefore these materials may also be prone to the formation of shear bands. Examples of this have been noted for Al-Mg-Si alloys (Liu and Doherty 1986) and for aluminium matrix particulate composites (Humphreys et al. 1990).

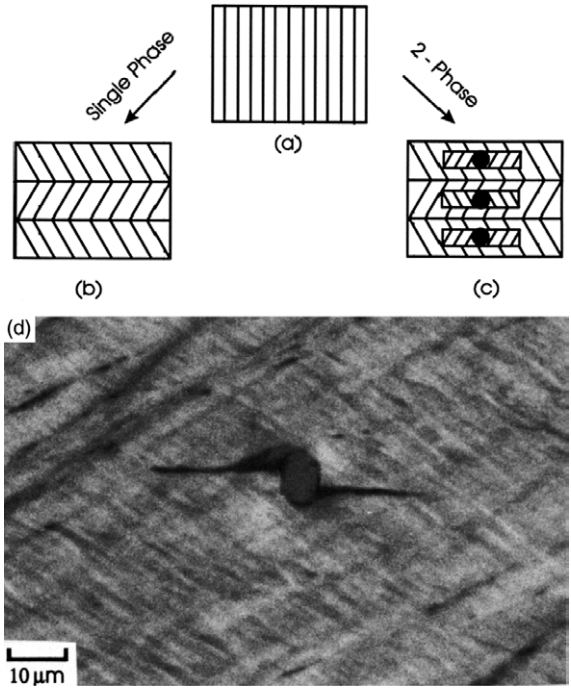

Fig. 2.31. The nucleation of deformation bands at particles. (a) Undeformed crystal of unstable orientation, (b) Formation of deformation bands in the deformed single-phase crystal, (c) Formation of small deformation bands at particles, (d) Optical micrograph showing deformation zone associated with a 10 μm particle in an Al–Si crystal of the same orientation, (Humphreys and Ardakani 1994).

2.9.3 Dislocation structures at individual particles

We have seen that second-phase particles affect the density and distribution of dislocations in the matrix, and that this may influence the driving force for recrystallization. In addition, we need to consider the accumulation of dislocations in the vicinity of large particles as this may lead to these regions becoming sites for recrystallization nucleation.

As discussed in §2.9.2, if the particles are strong enough to resist the passage of dislocations, then Orowan loops may be formed, and the stress on a particle from a single Orowan loop is given by equation 2.13. During continued deformation, more loops will form and the resulting stress will rapidly rise to a level where, if the particle does not deform, there will be local plastic flow or **plastic relaxation** in the matrix to relieve these stresses. Because of the high stresses associated with them, Orowan loops are very unstable and are rarely observed. The nature of this plastic

relaxation has been extensively studied for single crystals deformed to low strains, and to a much lesser extent in single crystals or polycrystals deformed to large strains. We are primarily interested here in those aspects of the deformation structures which are relevant to recrystallization, and for further details of the dislocation mechanisms the reader is referred to the reviews of Brown (1985) and Humphreys (1985).

For small particles and low strains, plastic relaxation generally involves the generation of prismatic dislocation loops, which are of lower energy than Orowan loops. These may be prismatic loops of the same Burgers vector as the gliding dislocations (primary prismatic loops) or alternatively, secondary prismatic loops of a different Burgers vector may be generated. In deformed single crystals, rows of primary prismatic loops aligned with the particles are found as seen in figure 2.32. In polycrystals, although aligned rows of loops are not generally observed, there is evidence that prismatic loops are formed at the particles.

At larger strains and larger particles, more complex dislocation structures are formed, and these are often associated with local lattice rotations close to the particles (fig 2.33), and such regions are commonly termed **particle deformation zones.** The form and distribution of such dislocation structures at particles are primarily functions of the strain and the particle size, although other factors such as shape, interface strength and matrix are known to be important (see e.g. Humphreys 1985). The effect of strain and particle size on the relaxation mechanisms in aluminium single crystals is summarised in figure 2.34. The transition from the dislocation structures such as figure 2.32 which are considered as non-rotational or 'laminar plastic flow' to the particle deformation zones such as in figure 2.33, which can be considered to involve 'rotational plastic flow', is difficult to predict theoretically as it is on a scale which is midway between dislocation and continuum mechanics. Brown (1997), using a dislocation plasticity model, has

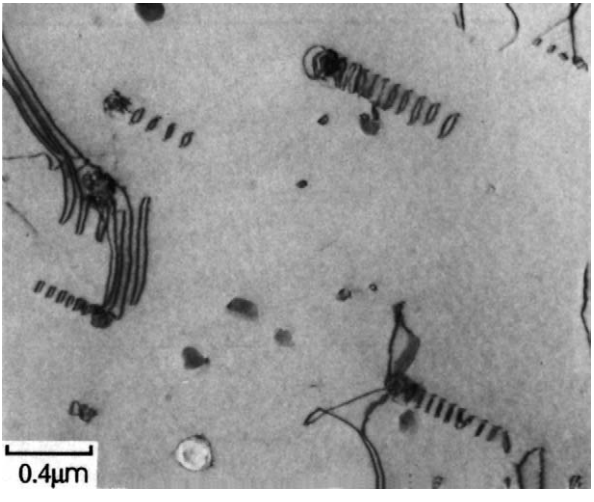

Fig. 2.32. Primary prismatic loops at Al_2O_3 particles in an α-brass crystal, (Humphreys 1985).

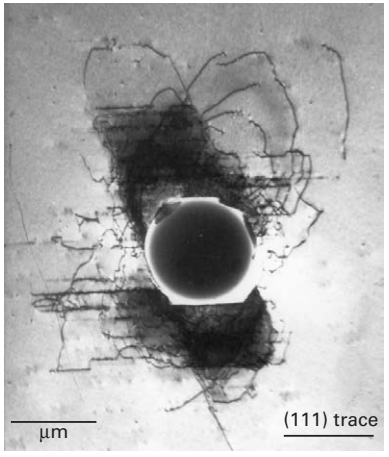

Fig. 2.33. Deformation zones at a silica particle above and below the primary slip plane, (111), in a deformed α-brass crystal. The primary Burgers vector is normal to the page, (Humphreys and Stewart 1972).

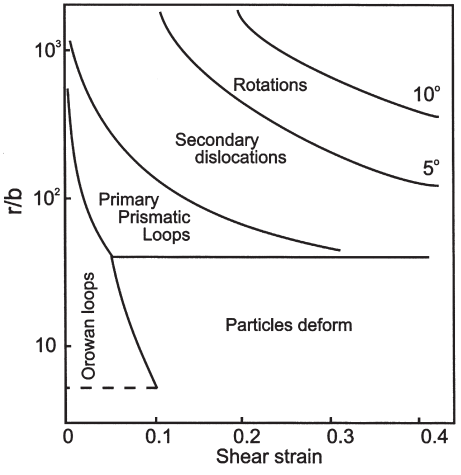

Fig. 2.34. Deformation mechanisms at particles in aluminium as a function of strain and normalised particle radius, (after Humphreys 1979a).

suggested that the transition at a particle of diameter d may occur at a shear strain (s) given by

$$s = \left(\frac{b}{d}\right)^3 \left(\frac{\sqrt{2}\alpha G}{\sigma_f}\right)^2 \tag{2.20}$$

where α is a constant of $\sim$0.5 and σ_f is the friction stress in the matrix.

The deformation zones formed at large particles are of particular interest as they are the source of particle stimulated nucleation of recrystallization (PSN) and may therefore have a strong influence on the grain size and texture after recrystallization.

2.9.4 Deformation zones at particles

Most of the detailed measurements of deformation zones at particles have been made on particle-containing single crystals oriented for single slip, and deformed in tension, although some information about the orientations within the deformation zones has been obtained from single crystals deformed in plane strain compression, and from deformed polycrystals.

2.9.4.1 Single crystals deformed in tension

In particle-containing single crystals of copper and aluminium, oriented for single slip, and deformed in tension (Humphreys 1979a) found that for particles of diameter less than 0.1 μm, deformation zones with local lattice rotations were not formed, and in such cases it was assumed that plastic relaxation occurred by the generation of prismatic loops as discussed above.

At larger particles, local lattice rotations were found to occur about the $<112>$ roller axis perpendicular to both the primary Burgers vector and the primary slip plane normal. The maximum rotation (θ_{max}) which was found to be close to the particle-matrix interface, and to decrease with distance (x) from the particle as shown in figure 2.35, dropped to a level indistinguishable from that of the matrix at distances of the order of the particle diameter ($x \sim d$). The data were found to fit an empirical

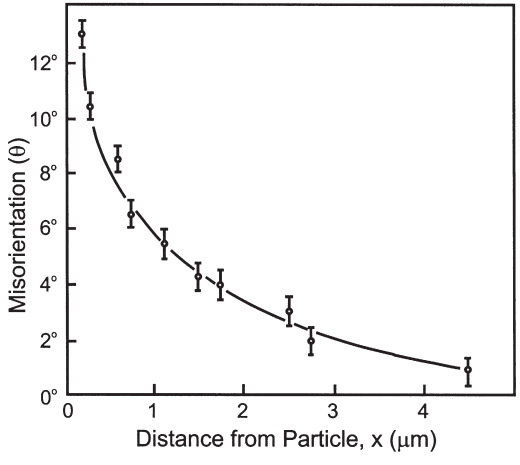

Fig. 2.35. Lattice misorientation at a 3 μm silicon particle in a deformed aluminium crystal as a function of distance from the interface, (Humphreys 1979a).

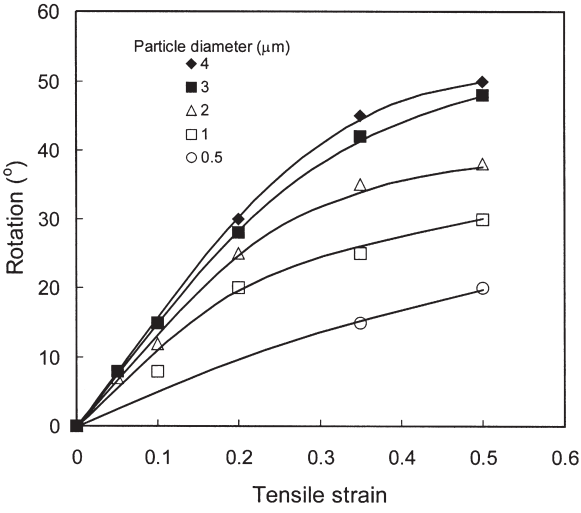

Fig. 2.36. The mean maximum misorientation at particles as a function of strain and particles size, (data from Humphreys 1979a).

equation of the form

$$\tan\theta = \tan\theta_{max}\exp\left(-\frac{c_1 x}{d}\right) \tag{2.21}$$

where c_1 is a constant equal to 1.8.

For particles of diameter greater than ~2.5 μm, θ_{max} was found to be a function only of the shear strain, s, (fig 2.36), indicating that lattice rotations were the only relaxation mechanism. The relationship between θ_{max} and s was of the form

$$\theta_{max} = c_2 \tan^{-1} s \tag{2.22}$$

where c_2 is a constant of the order of unity.

For particles in the size range 0.1 to ~2.5 μm, the maximum misorientation was a function of both strain and particle size as shown in figure 2.36, indicating that plastic relaxation occurred both by the formation of prismatic loops and rotated deformation zones. For such particles, the maximum misorientation (θ'_{max}) was found to fit the empirical equation

$$\theta'_{max} = 0.8\,\theta_{max}(d - 0.1)^{0.2} \tag{2.23}$$

where d is the particle diameter expressed in microns.

For elongated particles, it was found that the maximum misorientation occurred at the ends of the particle.

The detailed shape of the deformation zones described above was not determined, although the rotated regions tend to lie above and below the primary slip plane as seen in figure 2.33. In order to discuss recrystallization of the deformation zones in §9.3, it is convenient to have a semi-quantitative model of the zones, in which we assume that the zone is an 'onion skin' structure of concentric spherical low angle boundaries (fig 9.12). The distribution of dislocations in the deformation zone is directly related to the orientation distribution as given by equation 2.21.

The orientation gradient, $d\theta/dx$, at a distance x from the surface of the particle is given by

$$\frac{d\theta}{dx} = -\frac{c_1 \tan\theta_{max} \cos^2\theta}{d} \exp\left(-\frac{c_1 x}{d}\right) \tag{2.24}$$

and the dislocation density ρ, at distance x, assuming the low angle boundaries to comprise square networks of dislocations, is

$$\rho = \frac{2c_1 \tan\theta_{max} \cos^2\theta}{bd} \exp\left(-\frac{c_1 cx}{d}\right) \tag{2.25}$$

2.9.4.2 Single crystals deformed by plane strain compression or rolling

The microstructures of particle-containing aluminium single crystals of the following orientations, deformed in channel die plane strain compression have been investigated: $\{001\}<110>$ (Humphreys and Ardakani 1994), $\{011\}<100>$ (Ferry and Humphreys 1996b), $\{011\}<01\bar{1}>$ (Ferry and Humphreys 1996c). These have shown the rotations within the particle deformation zone to be related to the operating slip systems. The rotation axes are usually close to the transverse direction (TD), or to a nearby $<112>$ axis (see fig. 9.16a). These results are in agreement with those of the previous section, confirming that the subgrain size was considerably smaller in the deformation zones, that larger misorientations were found at the edges of platelike particles, and that the deformation zone typically extended for a distance of one particle diameter from the particle surface. Later investigations of rolled particle-containing aluminium crystals (Engler et al. 1999, 2001) have produced similar results.

2.9.4.3 Deformed polycrystals

There is little quantitative data for deformation zones in polycrystals mainly because of the severe experimental difficulties inherent in such measurements. The deformation zone in a rolled alloy is generally found to be elongated in the rolling direction as shown schematically in figure 2.37. Regions of highly misoriented small subgrains of diameter <0.1 μm are found close to the particle, but further away, the subgrains are elongated and distorted by the presence of the particle (Humphreys 1977, Hansen and Bay 1981). An example of the microstructure adjacent to large particles after cold rolling to a strain of 3.9, is shown in figure 14.4.

Few systematic studies of misorientations have been made, and it is commonly reported that even after large strains, the misorientation between the matrix and the deformation zone is of the order of 30°–40°, (e.g. Gawne and Higgins 1969, Humphreys 1977, Herbst

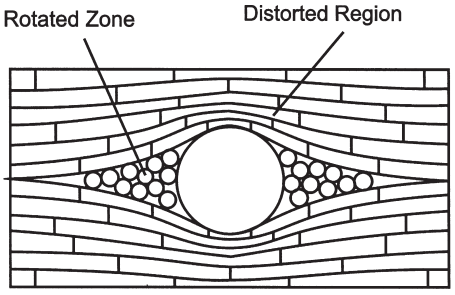

Fig. 2.37. A deformation zone in a rolled polycrystal, (after Porter and Humphreys 1979).

and Huber 1978, Bay and Hansen 1979, Liu et al. 1989). These misorientations were typically measured as **angle-axis pairs,** defined as the minimum angle of rotation (and the rotation axis) necessary to bring the crystals into register (§4.2). Because of the symmetry of cubic crystals, this is not necessarily the same as the **physical misorientation** which has occurred during deformation, and a mean misorientation of $\sim 40^\circ$ would be measured for **randomly** oriented crystals (§4.2). Therefore from such experimental measurements, we can only deduce that the physical misorientations are at least as large as the measured values, but because of the crystal symmetry they could be considerably larger.

A TEM microtexture technique in which the orientation spread within a small volume adjacent to a particle is measured (Humphreys 1983), has been used to investigate the misorientations within deformation zones at particles in polycrystalline aluminium deformed in uniaxial compression (Humphreys and Kalu 1990), and it was found that in many cases more than one deformation zone was formed per particle, and that the magnitude of the rotations increased with both strain and particle size. The recent development of High Resolution Electron Backscatter Diffraction (EBSD) has enabled the size, shape and orientation of deformation zones at particles in rolled polycrystals to be determined, and an example is shown in figure 2.38.

2.9.4.4 Modelling the deformation zone

The formation of a deformation zone at a micron-sized particle in a polycrystal during rolling is a process which occurs at a **scale which is difficult to model successfully.** The process is too complex to be analysed accurately in terms of individual dislocation reactions, whilst larger scale models such as finite element models have not been able to incorporate the subtle fine-scale size-dependent features of the deformation zones. Simple models based on dislocations and crystal plasticity have been proposed by Ashby (1966), Sandström (1980), Ørsund and Nes (1988), Humphreys and Kalu (1990) and Humphreys and Ardakani (1994). For the simplest case, of particles in a crystal deforming by single slip (§2.9.4.1), the best approach is currently the dislocation plasticity model of Brown (1997), which predicts that the misorientation in the deformation zone (θ) decreases with distance (x) from the particle of diameter d as

$$\tan\theta = -\frac{\tan(s)}{2}\ln\left(\frac{d}{x}\right) \tag{2.26}$$

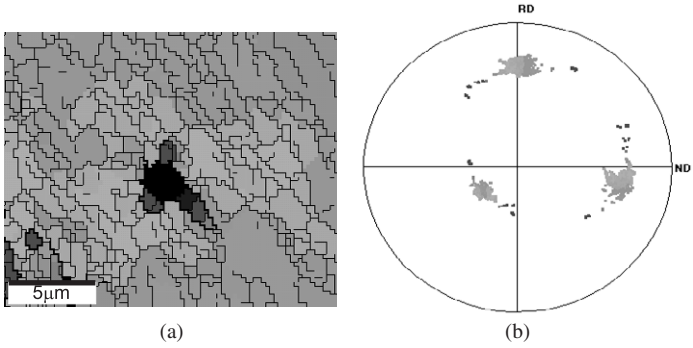

Fig. 2.38. EBSD measurement of misorientations at a 3 μm particle in an aluminium alloy (AA1200), cold rolled 75%. (a) EBSD map showing highly misoriented regions adjacent to the particle. (b) 100 pole figure of the area. The colours used for both map and pole figure represent rotations about the transverse direction (TD), blue in one direction and red in the other, with the matrix orientation green, (courtesy of A.P. Clarke). (See colour plate section).

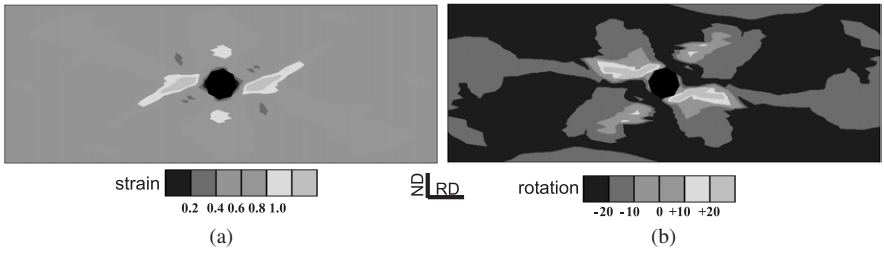

Fig. 2.39. Results of 2-D CPFEM simulation of plane strain deformation of a particle-containing $\{001\}<110>$ crystal deformed to a strain of 0.5 in plane strain compression. (a) von Mises effective strain, (b) crystal rotation about the constrained direction, in degrees (TD), (Humphreys and Bate 2002). (See colour plate section).

which gives a reasonable fit to the experimental data of Humphreys (1979a), as does the empirical equation 2.21. However, none of these models make a realistic attempt to predict the shape of the deformation zone.

For more complex situations, such as single crystals or polycrystals deformed in plane strain compression, some success has been achieved by incorporating **crystal plasticity into finite element models (CPFEM)** (Bate 1999). Figures 2.39a and b show the strain and orientation distributions predicted for a crystal of aluminium of initial orientation $\{001\}<110>$ deformed to a strain of 0.5, which was the case examined experimentally by Humphreys and Ardakani (1994). There is a good general agreement between the model (fig. 2.39b) and experiment (shown in fig. 2.31c), with the two 'plumes' of material near the particle rotating in the opposite sense to the matrix, toward the complementary 'copper' orientation.

The main drawback of such models is their **lack of a length scale,** i.e., the particles could be of any size, whereas in reality, it is known that there is a strong size effect for smaller particles as shown in figures 2.34 and 2.36. Gradient plasticity has been incorporated into finite element models in order to introduce a length scale (Fleck and Hutchinson 1994, Bassani 2001). However, incorporation of gradient plasticity into the CPFEM modelling of deformation at particles as described above, has been shown to have only a small effect on the results (Humphreys and Bate 2002), and has not predicted the reduction in the extent or magnitude of the deformation zones for small particles, which is found experimentally.

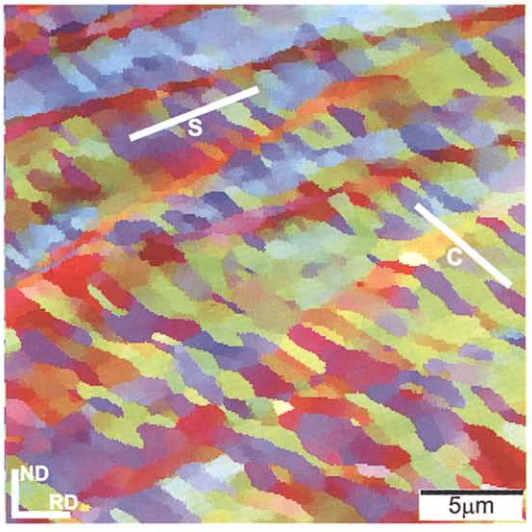

Fig. 2.12(b). See p. 33.

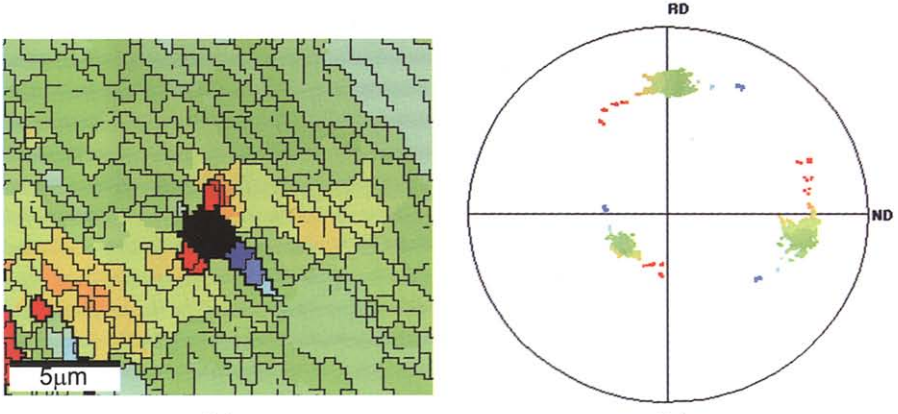

(a) (b)

Fig. 2.38. See p. 64.

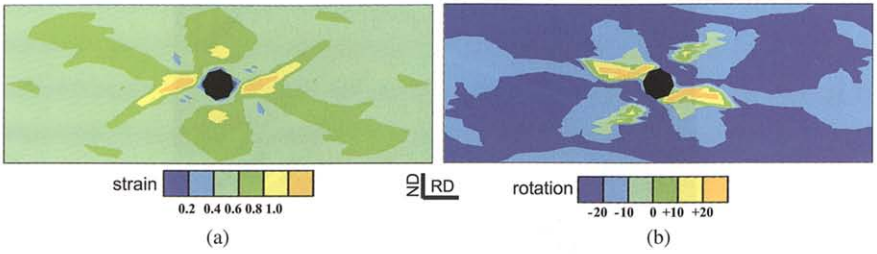

Fig. 2.39. See p. 64.

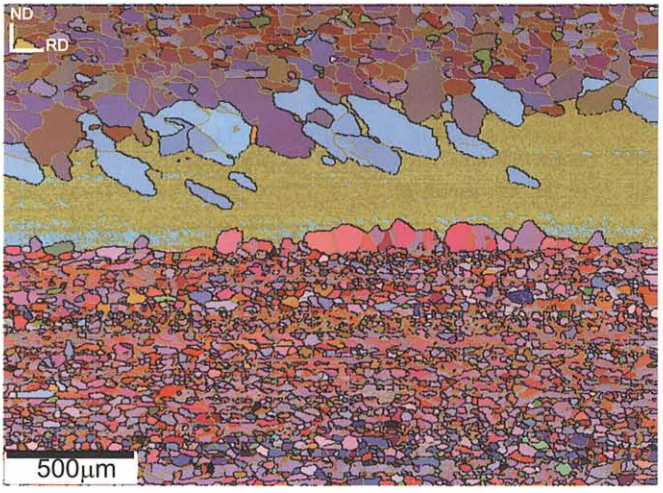

Fig. 7.15. See p. 240.